

Endothelial Nitric Oxide Synthase Activation Generates an Inducible Nitric Oxide Synthase-Like Output of Nitric Oxide in Inflamed Endothelium\*

Jessica L. Lowry<sup>1</sup>, Viktor Brovkovich<sup>1</sup>, Yongkang Zhang<sup>1</sup> & Randal A. Skidgel<sup>1,2</sup>

<sup>1</sup>From the Department of Pharmacology and <sup>2</sup>Center for Lung and Vascular Biology, University of Illinois College of Medicine, Chicago, Illinois 60612, USA

Running title: *eNOS Masquerades as iNOS in Inflamed Endothelium*

To whom correspondence should be addressed: Randal A. Skidgel, Department of Pharmacology (m/c 868), University of Illinois College of Medicine, 835 S. Wolcott, Chicago, IL 60612. Tel.: (312) 996-9179; Fax: (312) 996-1225; E-mail: rskidgel@uic.edu

**Key words:** inflammation; eNOS; JNK; cell migration; bradykinin

---

**Background:** In healthy endothelium, agonist-induced eNOS activation results in transient, calcium-dependent NO production.

**Results:** In inflamed endothelium, bradykinin stimulates prolonged eNOS-derived NO that depends on G $\alpha$ <sub>i</sub>, MEK1/2 and JNK, resulting in reduced migration.

**Conclusion:** eNOS activation is mediated differently in normal and inflamed endothelium, resulting in divergent NO production and effects.

**Significance:** High eNOS-derived NO may impair angiogenesis and wound healing in inflammation.

#### SUMMARY

High levels of NO generated in the vasculature under inflammatory conditions are usually attributed to inducible nitric oxide synthase (iNOS), but the role of the constitutively expressed endothelial NOS (eNOS) is unclear. In normal human lung microvascular endothelial cells (HLMVEC), bradykinin (BK) activates kinin B2 receptor (B2R) signaling that results in Ca<sup>2+</sup>-dependent activation of eNOS and transient NO. In inflamed HLMVEC (pretreated with interleukin-1 $\beta$  and interferon- $\gamma$ ), we found enhanced binding of eNOS to calcium-calmodulin at basal Ca<sup>2+</sup> levels, thereby increasing its basal activity that was

dependent on extracellular L-Arg. Furthermore, B2R stimulation generated prolonged high output eNOS-derived NO that is independent of increased intracellular Ca<sup>2+</sup> and is mediated by a novel G $\alpha$ <sub>i</sub>, MEK1/2 and JNK1/2-dependent pathway. This high output NO stimulated with BK was blocked with B2R antagonist, eNOS siRNA or eNOS inhibitor but not iNOS inhibitor. Moreover, B2R-mediated NO production and JNK phosphorylation were inhibited with MEK1/2 and JNK inhibitors or MEK1/2 and JNK1/2 siRNA but not with ERK1/2 inhibitor. BK induced Ca<sup>2+</sup>-dependent eNOS phosphorylation at Ser<sup>1177</sup>, Thr<sup>495</sup> and Ser<sup>114</sup> in cytokine-treated HLMVEC but these modifications were not dependent on JNK1/2 activation and were not responsible for prolonged NO output. Cytokine treatment did not alter the expression of B2R, G $\alpha$ <sub>q/11</sub>, G $\alpha$ <sub>i1,2</sub>, JNK or eNOS. B2R activation in control endothelial cells enhanced migration, but in cytokine-treated HLMVEC it reduced migration. Both responses were NO-dependent. Understanding how JNK regulates prolonged eNOS-derived NO may provide new therapeutic targets for the treatment of disorders involving vascular inflammation.

Nitric oxide (NO)<sup>3</sup> is synthesized by three isoforms of nitric oxide synthase (NOS): neuronal NOS (nNOS; NOS1), inducible NOS (iNOS; NOS2) and endothelial NOS (eNOS; NOS3).

nNOS and eNOS are constitutively expressed and require increased intracellular  $\text{Ca}^{2+}$  ( $[\text{Ca}^{2+}]_i$ ) for activation whereas iNOS expression is induced in response to inflammatory stimuli and once synthesized, is tightly bound to  $\text{Ca}^{2+}$ -calmodulin and is thereby constitutively active (1-3). The primary source of NO in the vasculature is eNOS under normal conditions, whereas iNOS becomes prominent under inflammatory conditions.

Nitric oxide can exert either beneficial or pathological effects on the cardiovascular system, dictated by the amount of NO produced, subcellular localization and protein interactions of NOS, in addition to the redox state of the cellular environment (4,5). Under physiological conditions, eNOS generates low levels of NO for maintenance of vascular homeostasis (6) and alterations in NO production contribute to the pathogenesis of vascular disorders such as hypertension, diabetes, heart failure and atherosclerosis (7).

Many vascular diseases are accompanied by inflammation, resulting in a general increase in NO production which, under conditions of oxidative stress, can lead to generation of peroxynitrite and protein nitration, DNA damage and apoptosis (8,9). Moreover, it is generally held that vascular inflammation leads to reduced bioavailability of eNOS-derived NO and eNOS “uncoupling”, accompanied by induction of endothelial iNOS expression, which is the source of high, uncontrolled NO that further exacerbates the disease process (10). However, we have found that iNOS activity in inflamed human endothelium can be increased 3- to 5-fold beyond its basal level by G protein-coupled receptor (GPCR) signaling (11-13) and accumulating evidence indicates that eNOS could also play an “iNOS”-type role in inflammation, but the mechanisms have not been defined (14).

The kallikrein-kinin system plays a prominent role in vascular inflammation and its biological effects are mediated by release of kinin peptides that activate two different G protein-coupled receptors named B1 (B1R), whose expression is induced by inflammatory mediators, and B2 (B2R), which is constitutively expressed (15,16). The B2R is selectively activated by bradykinin (BK) or kallidin (KD; Lys-BK) which can be further processed by plasma carboxypeptidase N (CPN) or membrane carboxypeptidase M (CPM) to generate

des-Arg<sup>9</sup>-BK or des-Arg<sup>10</sup>-KD which no longer activate the B2R, but instead are specific B1R agonists (16-18). Stimulation of the B2R or B1R differentially activates eNOS or iNOS respectively (19). In healthy endothelium, the kinin B2 receptor activates eNOS resulting in a short burst of  $\text{Ca}^{2+}$ -dependent NO production (20,21). Under inflammatory conditions, endothelial B1R stimulation leads to acute activation of iNOS via ERK1/2-dependent phosphorylation at Ser<sup>745</sup> and prolonged and high output NO production (11-13). However, signaling pathways for endothelial B2R-dependent NO production under inflammatory conditions have not been investigated.

Increased  $\text{Ca}^{2+}$ -calmodulin binding is a major mechanism for eNOS activation, but several other post-translational modifications govern its activity, including lipid attachment, phosphorylation, and S-nitrosylation (22,23). Phosphorylation modulates eNOS activity by altering enzyme localization, facilitating protein-protein interactions or inducing conformational changes that abet or impede efficient flow of electrons between the reductase and oxygenase domains (23,24). The best characterized phosphorylation sites on eNOS modified in response to BK (and many other agonists) stimulation in control endothelial cells include dephosphorylation of the inhibitory p-Thr<sup>495</sup> by calcineurin and phosphorylation at the stimulatory Ser<sup>1177</sup> by Akt (primarily) and also protein kinase A (PKA) and calcium-calmodulin-dependent kinase II (CaMKII) (25,26). Additionally, B2R activation alters phosphorylation at Tyr<sup>81</sup>, Ser<sup>615</sup> and Ser<sup>633</sup> but not Ser<sup>114</sup> (27-29).

In the present study, we discovered that B2R stimulation in cytokine-treated human lung microvascular endothelial cells (HLMVEC) induced prolonged high output NO by activating eNOS. Similar to iNOS, we found that eNOS binds calcium-calmodulin at basal  $\text{Ca}^{2+}$  levels in cytokine-treated endothelial cells, enhancing its basal activity and priming it for activation independent of increased  $[\text{Ca}^{2+}]_i$ . While BK-induced  $\text{Ca}^{2+}$  mobilization is critical for eNOS activation in healthy endothelium, we found that BK stimulates a novel  $\text{G}\alpha_{i/o}$ -mediated and MEK1/2  $\rightarrow$  JNK1/2-dependent activation of eNOS in inflamed endothelium. Moreover, we established that prolonged B2R-mediated NO production reduced endothelial cell migration, a

response opposite to that generated by B2R activation and NO production in control endothelial cells.

## EXPERIMENTAL PROCEDURES

**Materials**—Bradykinin (BK; RPPGFSPFR), bradykinin pseudopeptide analog ([Phe<sup>8</sup>ψ(CH-NH)-Arg<sup>9</sup>]-BK), 2-aminoethoxydiphenyl-borane (2-APB), tempol, MEK1/2 inhibitor U0126 and its corresponding negative control U0124 were from Tocris Bioscience/ R&D Systems, Inc. (Minneapolis, MN). Des-Arg<sup>10</sup>-kallidin (DAKD), calcium ionophore (A23187), icatibant acetate (HOE-140), des-Arg<sup>10</sup>-Leu<sup>9</sup>-kallidin (DALKD) and polyethylene glycol superoxide dismutase (PEG-SOD) were from Sigma-Aldrich (St. Louis, MO). NOS inhibitors (L-N<sup>G</sup>-nitro-L-arginine (L-NNA), 1400W, N<sup>W</sup>-propyl-L-arginine and the Nitrate/Nitrite Fluorometric Assay Kit (#780051) were from Cayman Chemicals (Ann Arbor, MI). DL-2-Mercaptomethyl-3-guanidinoethyl-thiopropionic acid (MGTA), BAPTA-AM, Akt inhibitor II SH-6, EGF receptor tyrosine kinase inhibitor PD153035, JNK Inhibitor II, JNK Inhibitor VIII, ERK Inhibitor II (FR180204) and ERK Inhibitor II negative control (FR180289) were from Calbiochem/ EMD Millipore (Billerica, MA). MEK1/2 inhibitors CI-1040 (PD184352) and PD98059 were from Selleck Chemical (Houston, TX) and Cell Signaling Technology (Danvers, MA), respectively. Pertussis toxin was from List Biological Laboratories (Campbell, CA). Antibodies to human eNOS, eNOS(pThr495), eNOS(pSer633) and nNOS were from BD Transduction Laboratories (San Jose, CA), rabbit anti-iNOS (H-174) was from Santa Cruz Biotechnology (Santa Cruz, CA) and bovine eNOS(pSer617) and eNOS(pSer116) were from Upstate Cell Signaling Solutions (Lake Placid, NY). Antibodies to human eNOS(pSer117), total-SAPK/JNK, phospho-SAPK/JNK (T183/Y185), p44/42 MAPK, phospho-p44/42 MAPK (T202/Y204), total-MEK1/2 and phospho-MEK1/2 (S217/S221) were from Cell Signaling Technology (Danvers, MA). Rabbit polyclonal antibodies to Gα<sub>i1,2</sub> and anti-Gα<sub>q/11</sub> were from Sigma-Aldrich (St. Louis, MO) and anti-β-actin and anti-glyceraldehyde-3-phosphate dehydrogenase (GAPDH) antibodies were from Ambion/ Life Technologies (Grand Island, NY). Mouse

monoclonal anti-calmodulin antibody (05-173) was purchased from Millipore (Temecula, CA).

**Cell Culture and Transfection**—Human lung microvascular endothelial cells (HLMVEC) from Clonetics were used from passage 4-6 and were cultured in dishes pre-coated with 0.1% (v/v) gelatin using endothelial cell basal medium-2 supplemented with growth factors from EGM-2 MV Bullet kit (Lonza; Walkersville, MD), 10% (v/v) fetal bovine serum (FBS), and 1% (v/v) penicillin-streptomycin solution (Cellgro; Manassas, VA). Human embryonic kidney (HEK293) cells from ATCC (Manassas, VA) were cultured in low glucose Dulbecco's Modified Eagle Medium (DMEM) (GIBCO/ Life Technologies; Grand Island, NY) supplemented with 10% (v/v) FBS and 1% (v/v) penicillin-streptomycin solution. HEK293 cells were transiently transfected using Effectene (Qiagen; Valencia, CA) reagent according to the manufacturer's instructions. Unless otherwise indicated, all experiments using HLMVEC or HEK293 cells were performed in phenol-red-free DMEM Nutrient Mix F-12 (Ham) from GIBCO/ Life Technologies (Grand Island, NY), supplemented with 0.5% (v/v) FBS.

**Cytokine treatment**—HLMVEC or HEK293 cells were treated with 5 ng/ml interleukin-1β (IL-1β) (Calbiochem/ EMD Millipore; Billerica, MA) and 100 U/ml interferon-γ (IFN-γ) (Invitrogen/ Life Technologies; Grand Island, NY) for 16-24 h to stimulate inflammation. Because cytokine treatment induces expression of kinin B1 receptors (B1R) and carboxypeptidase M (CPM), which can convert BK to the B1R agonist des-Arg<sup>9</sup>-BK, cells were routinely pretreated with B1R antagonist DALKD (1 μM) and CPM inhibitor MGTA (20 μM) for 30 min to block the B1R pathway, unless otherwise indicated.

**RNA Interference**— Small interfering RNA (siRNA) from Sigma-Aldrich (St. Louis, MO) was synthesized using previously published and validated sequences for eNOS (30), MEK1 (31), MEK2 (31), and JNK1/2 (32). Sequences (sense) are as follows: eNOS 5'-GGUCUGCACA-GGAAAUGUU[dT][dT]-3'; MEK1-:5'-AAGUC-CUGAAGAAAGCUGGAA-[dT][dT]-3'; MEK2-5'-AAGUCGGCGAACUCAAGA-C[dT][dT]-3'; JNK1/2 - 5'TGAAAGAATGTCCTACCTT-[dT][dT]-3'. Scrambled RNA duplex (sc-37007)

was from Santa Cruz Biotechnology and used as a negative control. HLMVEC were electroporated with 100 nM siRNA using the Amaxa Biosystems Nucleofector system (Lonza; Walkersville, MD) based on the manufacturer's kit and protocol (S005) optimized for HLMVEC. Cells were treated with cytokines 48-72 h later. Approximately 72-96 h post-transfection, total cell lysates were collected and protein knockdown efficiency was assessed by Western blot analysis.

**Western Blotting**—HLMVEC were washed once with ice-cold phosphate buffered saline (PBS) containing 1 mM Na<sub>3</sub>VO<sub>4</sub>. Cells were then lysed in ice-cold 2x Laemmli buffer (0.125 M Tris-HCl, pH 6.8, 20% (v/v) glycerol, 4% (w/v) SDS, 0.004% (w/v) bromophenol blue) supplemented with fresh 3% (v/v) β-mercaptoethanol, 1 mM Na<sub>3</sub>VO<sub>4</sub>, 20 mM β-glycerophosphate, 1 mM phenylmethylsulfonyl fluoride (PMSF), and 1% (v/v) protease inhibitor solution (Sigma-Aldrich; St. Louis, MO). HEK293 cells were washed once with ice-cold PBS containing 1 mM Na<sub>3</sub>VO<sub>4</sub> and lysed with ice-cold buffer containing 50 mM Tris-HCl, pH 7.6, 150 mM NaCl, 5 mM EDTA, 10% (v/v) glycerol, 1% (v/v) Triton X-100, 0.1% (w/v) SDS and 0.5% (w/v) sodium deoxycholate supplemented with fresh 3% (v/v) β-mercaptoethanol and inhibitors as stated above. Cells were lysed on ice for 30 min, collected and centrifuged at 14,000 x g for 15 min at 4°C. Cell lysates were separated on 10% SDS-PAGE gels and electrophoretically transferred to Immobilon PVDF membranes (EMD Millipore; Billerica, MA). Blots were blocked with 5% (w/v) evaporated nonfat milk in PBS containing 0.1% (v/v) Tween-20 and then incubated with the appropriate primary antibodies followed by horseradish peroxidase-labeled secondary antibody and the bands were visualized by enhanced chemiluminescence (Pierce/ Thermo Scientific; Rockford, IL).

**Co-immunoprecipitation Assay**—Control and cytokine-treated HLMVEC (~2.5x10<sup>6</sup> cells per condition; not stimulated with BK) were washed once with ice-cold PBS containing 1 mM Na<sub>3</sub>VO<sub>4</sub> and lysed with ice-cold buffer (500 μl) containing 25 mM HEPES (pH 7.7), 0.3 M NaCl, 1.5 mM MgCl<sub>2</sub>, 0.2 mM EDTA, 1% (v/v) Triton X-100, supplemented with fresh 1 mM dithiothreitol (DTT), 1 mM Na<sub>3</sub>VO<sub>4</sub>, 20 mM β-

glycerophosphate, 1 mM PMSF and 1% (v/v) protease inhibitor solution. Lysates were collected and centrifuged at 14,000 x g for 10 min at 4°C. eNOS was precipitated from the supernatant by rotating at 4°C with 6 μg of rabbit anti-eNOS antibody for 12-16 h followed by pull down with protein G Sepharose beads Sigma-Aldrich (St. Louis, MO) that were added 2 h before the end of the incubation period. Samples were resolved on a 4-20% mini-PROTEAN® TGX™ precast gel (Bio-Rad; Richmond, CA) and calmodulin was detected by immunoblotting with mouse anti-calmodulin antibody.

**NO measurements**—Cells were incubated in phenol-red-free DMEM/F-12 supplemented with 0.5% (v/v) FBS containing 1 μM DALKD and 20 μM MGTA for 30 min prior to addition of 100 nM BK or 100 nM BK-analog. Basal NOS activation was accessed by incubating cells in L-Arg-free DMEM/F-12 medium (without FBS) for 2 h prior to stimulation with 1 mM L-Arg. To directly measure NO production in real time, a highly sensitive porphyrinic microsensor was positioned with a micromanipulator close to the cell culture surface (20 ± 1 μm) and used as previously described (21,33). A computer-based Gamry VP600 potentiostat was used to measure the current generated, which was proportional to the NO released. Each electrode used was calibrated with NO standard. The concentration of NO achieved at max. (control cells) or 20 min (cytokine-treated cells) after addition of agonist was used to quantitate the results.

**Nitrate/Nitrite Fluorometric Assay**—Control and cytokine-treated HEK-B2R/eNOS cells (~2.5x10<sup>6</sup> cells/ml) were washed twice with pre-warmed HBSS (GIBCO 14025) and then incubated with HBSS containing 1 mM L-Arg, 4 μM 1400W, 1 μM DALKD and 20 μM MGTA. Cells were allowed to equilibrate for 10 min at 37°C prior to collecting the first aliquot (Time, 0 min) of HBSS. Removed HBSS was replenished and cells were then stimulated with vehicle (HBSS) or 1 μM BK. Post-BK stimulation (60 min), HBSS was collected and centrifuged at 250 g for 10 min to remove potential cell debris. NO<sub>2</sub><sup>-</sup>/NO<sub>3</sub><sup>-</sup> accumulation present in 20 μl of HBSS was detected by following the manufactures instructions (Cayman Chemicals; Ann Arbor, MI). In brief, 2,3-diaminonaphthalene (DAN) reacts

with nitrite ( $\text{NO}_2^-$ ) yielding the fluorescent product, 1(H)-naphthotriazole, which is detected with a plate reader capable of measuring fluorescence using an excitation wavelength of 365 nm and an emissions wavelength of 430 nm. Because the DAN reagent only reacts with  $\text{NO}_2^-$ , nitrate ( $\text{NO}_3^-$ ) was converted to  $\text{NO}_2^-$  by incubating samples with nitrate reductase for 1 h at room temperature. To determine BK-induced  $\text{NO}_2^-/\text{NO}_3^-$  accumulation, basal  $\text{NO}_2^-/\text{NO}_3^-$  accumulation was subtracted from the BK-stimulated conditions.

**$\text{Ca}^{2+}$  Measurements**—Increased  $[\text{Ca}^{2+}]_i$  was measured with the  $\text{Ca}^{2+}$ -sensitive fluorescent probe fura-2/AM as described (18) with minor modifications. Control and cytokine-treated HLMVEC were grown to confluence on glass coverslips and then incubated for 45 min at 37°C in phenol-red free DMEM/F-12 medium containing 10% (v/v) FBS and 2.5  $\mu\text{M}$  fura-2AM. After loading, cells were washed and mounted at room temperature in a Sykes-Moore chamber on an inverted microscope coupled to the Attofluor Ratiovision. Fura-2 fluorescence was excited at 340 and 380 nm and the ratio of the resulting intensities at 510 nm was measured. Ionophore was routinely used as positive control. The tracings show mean values obtained with the simultaneous measurement of changes in the  $[\text{Ca}^{2+}]_i$  level in 10 to 30 cells.

**Quantitative Real Time-PCR (qRT-PCR)**—Total RNA was extracted from  $2.5 \times 10^6$  cells from control and cytokine-treated HLMVEC using the TRIzol® Reagent (Invitrogen/ Life Technologies; Grand Island, NY) according to the manufacturer's instructions. Using 5  $\mu\text{g}$  isolated RNA, reverse transcription was performed with the SuperScript First-Strand Synthesis System for RT-PCR according to Invitrogen's protocol. PCR was made in a 50  $\mu\text{l}$  reaction volume using a 96-well plate format containing 25  $\mu\text{l}$  Platinum® SYBR® Green qPCR SuperMix-UDG, 1  $\mu\text{l}$  ROX reference dye, 0.5  $\mu\text{g}$  cDNA template, 1  $\mu\text{l}$  of 10  $\mu\text{M}$  forward and reverse primer and 20  $\mu\text{l}$  of DEPC-treated water. Three replicate wells were taken for each target gene. Integrated DNA Technology synthesized the primers and sequences are as follows: B2R forward 5'-GGTGGGGACGGTGGGGACAT-3' and reverse 5'-AGCCACTCCACTTGG GGGCA -3' (34); B1R forward 5'-GAAGTGCAGTGGCACAAT-

CATAG-3' and reverse 5' GCCCAAG ACA-AACACCAGAT-3'; GAPDH forward 5'-TCG-AGACCATCTTCCAGGAG-3' and reverse 5'-ACAGCCTTGGCAGCAC-CAGT-3'.

Quantitative real-time PCR was performed in an Applied Biosystems 7000 system following a standard cycling program for ABI Instruments. Briefly, stage 1 consisted of UDG incubation at 50°C for 2 min, stage 2 was set at 95°C for 2 min, followed by stage 3 consisting of 40 cycles of denaturation at 95°C for 15 s and annealing at 60°C for 30 s. No amplification signals were detected when reverse transcription was omitted for all probes (data not shown). mRNA expression levels were compared by the comparative  $\Delta\Delta C_T$  method, using the level of GAPDH mRNA as a calibrator.

**Wound healing assay**—Wound healing was assessed using the *in vitro* scratch assay technique as previously described (35). Briefly, a cell-free zone, within a confluent monolayer of control or cytokine-treated HLMVEC, was formed down the center of a 6-well tissue-culture dish by removing cells with the pointed end of a sterile 200  $\mu\text{l}$  pipette tip. Cells were then washed 2x with serum-free media and sustained in growth factor-free EBM-2 medium supplemented with 10% (v/v) FBS, 1  $\mu\text{M}$  DALKD, 20  $\mu\text{M}$  MGTA, without or with 10  $\mu\text{M}$  HOE-140, 4  $\mu\text{M}$  L-NNA or 10  $\mu\text{M}$  tempol. Using phase contrast microscopy, 5-10 distinct images of unstimulated cells along the cell-free zone were taken and the coordinates were documented. Thereafter, cells were stimulated with 1  $\mu\text{M}$  BK or 15  $\mu\text{l}$  vehicle (basal DMEM/F-12 medium) and images were collected 12 h later at the original coordinates. Wound closure was quantified by measuring the area of the cell-free zone before and 12 h after BK-stimulation. Using Image J software, % wound closure was calculated as  $[\Delta \text{Area of wound } (T_{\text{Initial}} - T_{\text{Final}}) / \text{Area of wound at } T_{\text{Initial}}] \times 100$ .

**Apoptosis Assay**—Apoptosis was evaluated using the *in situ* cell death detection kit (Roche; Indianapolis, IN) according to manufacturer's instructions. Cytokine-treated HLMVEC were grown to confluence on glass coverslips. Samples were incubated for 20 min in DMEM/F-12 medium supplemented with 10% (v/v) FBS, 20  $\mu\text{M}$  MGTA and 10  $\mu\text{M}$  DALKD, followed by a 12 h incubation with or without 1  $\mu\text{M}$  BK. Medium

was then carefully removed and cells were air-dried. Coverslips were not rinsed with PBS to prevent inadvertent removal of apoptotic cells. Next, samples were fixed with 4% (v/v) paraformaldehyde in PBS (pH 7.4), permeabilized with 0.1% (v/v) Triton X-100 in 0.1% (w/v) sodium citrate solution and then treated with TUNEL reaction mixture consisting of enzyme solution and label solution provided by the manufacturer. The positive control sample was treated with 50 U/ml of recombinant DNase I prior to labeling, while the negative control consisted of cells treated in the absence of terminal transferase (enzyme solution). Coverslips were then rinsed with H<sub>2</sub>O, air-dried and prepared with ProLong® Gold antifade mounting reagent containing DAPI (Invitrogen/ Life Technologies; Grand Island, NY). Lastly, samples were analyzed with a Zeiss ApoTome microscope using an excitation wavelength in the range of 450-500 nm and detection in the range of 515-565 nm.

*Modified Boyden Chamber Assay*—Endothelial transmigration was performed using 24-well Millicell® hanging cell culture inserts containing PET membranes with 8.0 µm pores (Millipore; Billerica, MA). Briefly, membranes were pre-coated overnight with 0.1% (v/v) gelatin and then air-dried. The bottom wells were filled with EBM-2 medium supplemented with growth factors from EGM-2 MV Bullet kit and 10% (v/v) FBS and the Millicell® cell culture insert was inserted into the top. A cell suspension (~1.0x10<sup>5</sup> control or cytokine-treated HLMVEC in 400 µl of EBM-2 medium supplemented with 10% (v/v) FBS) without or mixed with agonist and/or inhibitors, was added to the top chamber. Transmigration through the membrane was allowed to proceed for 8 h at 37°C in a humidified atmosphere of 95% air and 5% CO<sub>2</sub>. The bottom surface of the membrane was then washed once with PBS and fixed with 4% (v/v) paraformaldehyde for 10 min at room temperature. Cells on the upper surface of the membrane were carefully removed with a cotton tip. The membranes were then excised from the insert, washed twice with H<sub>2</sub>O, air dried and mounted with ProLong® Gold antifade reagent with DAPI. Cells present on the lower surface of the membrane were counted under a Zeiss ApoTome microscope.

## RESULTS

*Kinin B2 receptor (B2R) activation generates prolonged NO production in inflamed endothelial cells* - B2R-mediated eNOS activation in bovine aortic endothelial cells and human umbilical vein endothelial cells has been well characterized (20,26). However, B2R-stimulated NO production has not been studied in endothelial cells under inflammatory conditions that are classically associated with activation of the kallikrein-kinin system and generation of B2R agonist kinins (15,16). To investigate this, human lung microvascular endothelial cells (HLMVEC) or human embryonic kidney cells transiently expressing B2R and eNOS (HEK-B2R/eNOS) were pretreated with 5 ng/ml of interleukin-1beta (IL-1β) and 100 U/ml of interferon-gamma (IFN-γ) for 16-24 h (“cytokine treated”). Unless otherwise indicated, cells were then pre-incubated for 30 min with B1R antagonist DALKD (1 µM) and carboxypeptidase inhibitor MGTA (20 µM). This pretreatment blocks B1R signaling by antagonizing the receptor and inhibiting the carboxypeptidase-mediated conversion of bradykinin (BK) to B1R agonist des-Arg<sup>9</sup>-BK (17,18,21). We found that stimulation of the B2R with 100 nM BK in control HLMVEC (Fig. 1A, *top*) or HEK-B2R/eNOS (Fig. 1B, *top*) resulted in transient NO, reaching a maximum at 5 min and returning to baseline in 10 min. However, in cytokine-treated HLMVEC (Fig. 1A, *top*) or cytokine-treated HEK-B2R/eNOS (Fig. 1B, *top*), BK induced higher and more prolonged NO, reaching a maximum in ~40 min and not returning to baseline until ~80 min.

To confirm that the prolonged NO response was mediated via B2R (and not B1R) activation, we used a pseudopeptide BK analog, [Phe<sup>8</sup>ψ(CH<sub>2</sub>-NH)Arg<sup>9</sup>]bradykinin, that has a non-peptide C-terminal bond (36). This BK analog cannot be cleaved by carboxypeptidases, thus preventing its conversion into a des-Arg<sup>9</sup> B1R agonist, allowing experiments to be done in the absence of DALKD and MGTA. As shown in Fig. 1C (*top*), BK analog also stimulated prolonged NO production in cytokine-treated HLMVEC. The response to BK (Fig. 1A, *bottom*) and BK analog (Fig. 1C, *bottom*) were both blocked with B2R antagonist HOE-140 (1 µM). Thus, prolonged NO stimulated

by BK in cytokine-treated HLMVEC depends on activation of the B2R and not the B1R.

Cellular NO consumption is an important factor regulating intracellular NO signaling (37,38). Because electrode-based measurements of NO detect changes from baseline, detection of increased NO could reflect either enhanced NO output by a NOS or a decrease in consumption of basally generated NO. As one way to address this, we used 2,3-diaminonaphthalene (DAN) to measure total nitrite ( $\text{NO}_2^-$ ) accumulation after conversion of nitrate ( $\text{NO}_3^-$ ) to  $\text{NO}_2^-$  with nitrate reductase. Cells were pre-incubated with iNOS inhibitor 1400W to block possible  $\text{NO}_3^-/\text{NO}_2^-$  generation by iNOS, whose expression is induced by cytokine treatment. We detected a significant increase in BK-stimulated  $\text{NO}_3^-/\text{NO}_2^-$  accumulation (after 60 min) in medium from cytokine-treated HEK-B2R/eNOS cells ( $64 \pm 15$  nM,  $n = 3$ ) whereas there was no detectable increase in  $\text{NO}_3^-/\text{NO}_2^-$  in control HEK-B2R/eNOS cells stimulated with BK, suggesting an increase in eNOS-derived NO under cytokine-treated conditions. For unknown reasons, the same assay did not give reproducible results in HLMVEC, so in these cells we used a previously published approach (37) using the long half-life (20h) NO donor DETA-NONOate to test whether BK stimulation results in decreased NO consumption. DETA-NONOate provides a constant source of NO which, after a few minutes of incubation with cells, rises to a plateau (as measured with a microelectrode) whose amplitude is inversely correlated with the rate of NO consumption and varies, depending on cell type (37). Cytokine-treated HLMVEC were pre-incubated with 4  $\mu\text{M}$  L-NNA and 4  $\mu\text{M}$  1400W to block eNOS and iNOS and then DETA-NONOate (5  $\mu\text{M}$ ) was added to the cells. NO, measured continuously with the microsensor, achieved a steady state concentration of  $\sim 260$  nM after  $\sim 8$  min. Addition of 100 nM BK at 10 min did not change the steady-state concentration of NO which, when measured at 20 min, was  $250 \pm 25$  nM with NO donor alone vs.  $275 \pm 20$  nM with NO donor + BK ( $n = 3$ ), indicating that BK stimulation does not inhibit NO consumption.

One other potential mechanism by which BK might increase NO is by enhancing nitrite reductase activity to convert  $\text{NO}_2^-$  to NO, which has also been reported to be catalyzed by eNOS,

although only under hypoxic and/or acidic conditions (39). To test this, cytokine-treated HLMVEC were pre-incubated in L-Arg-free medium (as 300  $\mu\text{M}$  L-Arg can inhibit eNOS nitrite reductase activity(39)) with 4  $\mu\text{M}$  1400W to block iNOS. Addition of 10  $\mu\text{M}$   $\text{NO}_2^-$  alone or 10  $\mu\text{M}$   $\text{NO}_2^-$  + 100 nM BK did not generate significant NO after 20 min as measured with the porphyrinic microsensor ( $10 \pm 10$  nM NO or  $15 \pm 15$  nM NO, respectively;  $n = 3$ ). Thus, the BK-stimulated NO response is not due to activation of nitrite reduction. It is of interest that the lack of a response in the absence of extracellular L-Arg is usually considered to be a property of iNOS regulation but not eNOS (40).

The above data support the conclusion that the prolonged NO output stimulated by BK-mediated B2R activation in cytokine-treated cells is due to increased NOS activity.

*Prolonged B2R-mediated NO production is mediated by eNOS activation* - We previously reported that in cytokine-treated HLMVEC, B1R activation results in post-translational activation of iNOS leading to very high and prolonged NO production (11,12). Interestingly, the time-course of B2R-mediated NO production in cytokine-treated HLMVEC (Fig. 1A, *top*) is strikingly similar to that generated by B1R-mediated activation of iNOS (11,12). However, the total NO released by B2R activation (based on area under the curve for the total NO response) was  $\sim 53\%$  of the B1R-stimulated iNOS response (11) in cytokine-treated HLMVEC ( $300 \pm 25$  area units for B1R/iNOS vs.  $160 \pm 20$  area units for B2R-stimulated NO;  $n = 3$ ). To determine which NOS isoform was being activated, we used L-NNA to inhibit eNOS and 1400W to inhibit iNOS. (Based on  $K_i$  values, L-NNA is  $\sim 100$ -fold more selective for eNOS/nNOS than iNOS, whereas 1400W is  $\sim 7000$ -fold more selective for iNOS than eNOS). Using the porphyrinic microsensor, B2R-mediated NO production was inhibited 60-80% by 4  $\mu\text{M}$  L-NNA, whereas 4  $\mu\text{M}$  1400W had only a minor effect in HLMVEC (Fig. 1A, *bottom*) and HEK-B2R/eNOS (Fig. 1B, *bottom*). Similar results were obtained with the BK analog [Phe<sup>8</sup> $\psi$ (CH<sub>2</sub>-NH)Arg<sup>9</sup>]bradykinin in the absence of DALKD and MGTA (Fig. 1C, *bottom*). NOS inhibitor selectivity was verified by stimulating receptor-independent NOS activity in human embryonic kidney (HEK) cells over-expressing either iNOS

or eNOS alone. We confirmed that 4  $\mu\text{M}$  L-NNA inhibited  $\text{Ca}^{2+}$  ionophore (10  $\mu\text{M}$  A23187) stimulated eNOS activity but not basal L-Arg-stimulated iNOS activity, whereas 4  $\mu\text{M}$  1400W inhibited L-Arg-stimulated iNOS activity but not A23187-stimulated eNOS activation (data not shown). When BK was used to stimulate HEK cells transfected with only the B2R (in the absence of eNOS) in both control and cytokine-treated cells, there was no NO response as detected with the porphyrinic microsensor, nor  $\text{NO}_3^-/\text{NO}_2^-$  accumulation measured with the DAN reagent (data not shown).

Because L-NNA can also inhibit nNOS, we explored whether B2R stimulation might activate nNOS in cytokine-treated HLMVEC. Although nNOS is typically localized in neuronal tissue, its expression was also reported in endothelial cells (41,42). First, we analyzed eNOS, iNOS and nNOS protein expression in total cell lysates collected from control and cytokine-treated HLMVEC. As shown in Fig. 2A, cytokine treatment increased expression of iNOS but did not alter eNOS or nNOS protein expression. We also measured BK-stimulated NO production from cytokine-treated HLMVEC pretreated with NOS inhibitor  $\text{N}^w$ -propyl-L-arginine (0.01-10  $\mu\text{M}$ ) which has ~8-fold selectivity for nNOS ( $K_i = 5$  nM) over eNOS ( $K_i = 39$  nM). As shown in Fig. 2B, substantial inhibition of B2R-mediated NO production was only seen with high concentrations of  $\text{N}^w$ -propyl-L-arginine (1 – 10  $\mu\text{M}$ ), consistent with suppression of eNOS activity.

To confirm that B2R-mediated NO production was derived from eNOS, we transfected HLMVEC with siRNA targeting human eNOS (30) followed by cytokine treatment. As shown in Fig. 2C, we achieved ~85% knockdown of eNOS expression and B2R-mediated NO production was reduced by 61% in cytokine-treated HLMVEC transfected with eNOS siRNA compared with cells transfected with non-specific control siRNA. The residual NO production was due to the remaining eNOS, as it was blocked by eNOS inhibitor (L-NNA) but not with iNOS inhibitor 1400W (Fig. 2C). Similar inhibition of NO production was obtained when we knocked down eNOS expression in control HLMVEC and used A23187 to stimulate receptor-independent eNOS activity (Fig. 2D). Overall, our data show that cytokine treatment induces B2R-mediated and eNOS-

dependent prolonged NO production.

*Cytokine treatment induces a time-dependent change in kinetics of B2R-mediated NO production*-Cytokines can alter cell functions by promoting changes in gene expression and protein synthesis over a time course of several hours (43). We previously showed that IL-1 $\beta$  and IFN- $\gamma$  increased expression of CPM, B1R and iNOS in HLMVEC (21,44). To determine if prolonged B2R-mediated NO production was acutely affected by cytokine treatment or required a prolonged incubation, we measured the kinetics of NO production in HLMVEC treated with IL-1 $\beta$  and IFN- $\gamma$  for 2, 6, 10 or 16 h prior to stimulation with 100 nM BK. As shown in Fig. 3, the kinetic profile of B2R-mediated NO production did not differ from untreated cells at 2 h, but noticeably changed 6 h post-cytokine treatment, resulting in two phases of NO production. The first peak is similar to that observed in untreated cells, reaching maximal NO levels in 5 min, but instead of returning to baseline, the initial rapid peak is superimposed on a slower developing second phase of NO production. Pretreatment with cytokines for 10 h or 16 h prior to BK stimulation almost eliminated the initial transient peak while leaving the prolonged phase intact.

*Divergent G protein-coupled signaling pathways mediate B2R-dependent eNOS activation in control and cytokine-treated HLMVEC*-The kinin B2R is a prototypical  $\text{G}\alpha_{q/11}$ -coupled receptor whose activation leads to stimulation of phospholipase C (PLC) and increased  $[\text{Ca}^{2+}]_i$ , but it can also couple through  $\text{G}\alpha_{i/o}$  (16,45). To determine whether  $\text{G}\alpha_{q/11}$ -mediated  $\text{Ca}^{2+}$  release was required for B2R-mediated eNOS activation, we measured NO production from control and cytokine-treated HLMVEC (Fig. 4A) and HEK-B2R/eNOS (Fig. 4B) pretreated with the  $[\text{Ca}^{2+}]_i$  chelator BAPTA-AM (25  $\mu\text{M}$ ) for 30 min. In control cells, B2R-mediated NO production was reduced by BAPTA-AM, consistent with a  $\text{G}\alpha_{q/11}$ -coupled response. In contrast, prolonged B2R-mediated NO production in cytokine-treated cells was not inhibited by 25  $\mu\text{M}$  BAPTA-AM using either BK (Fig. 4A) or  $[\text{Phe}^8\psi(\text{CH}_2\text{-NH})\text{Arg}^9]$ bradykinin (Fig. 4C) as agonist. However, the remaining small initial transient peak was blocked (Fig. 5A), indicating it is a remnant of the B2R response found in control

HLMVEC as indicated in Fig. 3. A higher concentration of BAPTA-AM (37.5  $\mu\text{M}$ ) was also ineffective in inhibiting prolonged B2R – mediated NO production in cytokine-treated HLMVEC (data not shown), and the response was unaffected by pretreatment with thapsigargin (2  $\mu\text{M}$ ) to deplete  $[\text{Ca}^{2+}]_i$  stores or a combination of BAPTA-AM and thapsigargin (Fig. 5B). Furthermore, the prolonged B2R-mediated response in cytokine-treated HLMVEC was still present in cells that were pre-incubated in  $\text{Ca}^{2+}$ -free media in the absence or presence of 2-aminoethoxydiphenyl borate (2-APB; 50  $\mu\text{M}$ ) to block the  $\text{IP}_3$  receptor (Fig. 5C). However, 2-APB did inhibit the initial small transient NO peak as seen with BAPTA-AM. These results show that in cytokine-treated HLMVEC, prolonged B2R-mediated eNOS activation is independent of increases in  $[\text{Ca}^{2+}]_i$  induced by either release from intracellular  $\text{Ca}^{2+}$  stores or extracellular  $\text{Ca}^{2+}$  influx.

To determine if the lack of inhibition of the NO response in cytokine-treated HLMVEC by BAPTA-AM was due to the inability of B2R activation to increase  $[\text{Ca}^{2+}]_i$ , we measured the increase in  $[\text{Ca}^{2+}]_i$  in response to BK. As shown in Fig. 5D, not only did BK increase  $[\text{Ca}^{2+}]_i$  in cytokine-treated HLMVEC, but the peak  $\text{Ca}^{2+}$  response was  $\sim 4.5$ -fold greater than in control HLMVEC. The increase in peak  $[\text{Ca}^{2+}]_i$  was not mediated by  $\text{G}\alpha_{i/o}$ -signaling as PTx did not inhibit the  $\text{Ca}^{2+}$  response in cytokine-treated HLMVEC (Fig. 5E). Thus, the lack of  $\text{Ca}^{2+}$ -dependence of the eNOS response to BK in cytokine-treated HLMVEC is not due to the inability of BK to stimulate increased  $[\text{Ca}^{2+}]_i$ .

To determine if the prolonged B2R-mediated NO response in cytokine-treated cells was dependent on coupling through  $\text{G}\alpha_{i/o}$ , we measured NO production from control and cytokine-treated HLMVEC pretreated with 1.5  $\mu\text{g/ml}$  pertussis toxin (PTx) for 3 h prior to stimulation with BK. As shown in Fig. 4A & 4B, PTx had no effect on B2R-mediated NO production in control HLMVEC or HEK-B2R/eNOS, but substantially inhibited the response in cytokine-treated cells, indicating that it is mediated by B2R coupling through  $\text{G}\alpha_{i/o}$ . PTx also inhibited the prolonged B2R-dependent NO stimulated by BK analog  $[\text{Phe}^8\psi(\text{CH}_2\text{-NH})\text{Arg}^9]$ bradykinin (Fig. 4C).

Because PI3K-mediated Akt activation is involved in the regulation of eNOS by many agonists, we measured the effect of Akt inhibitor SH-6 on B2R-mediated NO production from control and cytokine-treated HLMVEC (Fig. 4A) or HEK-B2R/eNOS (Fig. 4B). SH-6 (15  $\mu\text{M}$ ) significantly reduced B2R-mediated NO generation in control cells, but had no effect on cytokine-treated HEK-B2R/eNOS cells, and inhibited only  $\sim 20\%$  of the response in cytokine-treated HLMVEC. To further study the possible role of Akt in HLMVEC, we treated cells with a different highly specific and potent allosteric Akt inhibitor, MK2206 (5  $\mu\text{M}$ ) and found, as with SH-6, that it inhibited B2R-mediated NO generation in control cells, but this inhibitor had no effect in cytokine-treated HLMVEC (Fig. 4A), even at higher concentrations up to 50  $\mu\text{M}$  (not shown). Thus, the B2R-mediated NO response in cytokine-treated HLMVEC is independent of Akt activation.

*Effect of cytokine treatment on  $\text{Ca}^{2+}$ -CaM binding and basal eNOS activity* - Both eNOS and nNOS typically require an increase in intracellular  $\text{Ca}^{2+}$  for activation, whereas iNOS binds  $\text{Ca}^{2+}$ -CaM tightly at low basal  $\text{Ca}^{2+}$  levels and is therefore constitutively active (1-3). To determine if cytokine treatment enhances basal eNOS affinity for  $\text{Ca}^{2+}$ -CaM, we immunoprecipitated total eNOS from control and cytokine-treated HLMVEC and immunoblotted for co-immunoprecipitated CaM. Interestingly, there was a  $\sim 4$ -fold increase in  $\text{Ca}^{2+}$ -CaM association with eNOS in cytokine-treated cells compared with control cells (Fig. 6A). Total cell lysates collected from control and cytokine-treated HLMVEC indicated no difference in either eNOS or CaM protein expression.

Enhanced affinity for  $\text{Ca}^{2+}$ -CaM binding is responsible for constitutive iNOS activity, which depends on the presence of extracellular L-Arg (46). Because we found that BK did not stimulate increased NO in cytokine-treated HLMVEC in the absence of extracellular L-Arg either in the presence (see above) or absence (not shown) of extracellular  $\text{NO}_2^-$ , we wondered whether increased  $\text{Ca}^{2+}$ -CaM binding would result in enhanced basal L-Arg-dependent eNOS-derived NO, similar to that found with iNOS. To assess this, we depleted control and cytokine-treated HLMVEC of L-Arg and then added back 1 mM L-Arg to stimulate basal NOS activity (Fig. 6B). As previously shown (11), L-Arg stimulated basal

iNOS-derived NO production in cytokine-treated HLMVEC which was significantly inhibited by the iNOS-selective inhibitor 1400W. However, there remained a substantial NO response that was almost completely inhibited by the further addition of eNOS inhibitor L-NNA (Fig. 6B). Conversely, in control HLMVEC (which express low levels of iNOS; Fig. 2A) basal eNOS activity was not detectable as L-Arg stimulated a smaller NO response that was inhibited by iNOS inhibitor 1400W, but not by eNOS inhibitor L-NNA (Fig. 6B). Thus, eNOS-derived NO can be generated by the addition of extracellular L-Arg and is consistent with our finding of enhanced eNOS binding to  $\text{Ca}^{2+}$ -CaM at basal  $\text{Ca}^{2+}$  levels in cytokine-treated endothelial cells.

*Effect of cytokine treatment on B2R and G protein expression* - Typically, B2Rs are constitutively expressed whereas B1R expression is induced by inflammatory cytokines (16). However, IL-1 $\beta$  was reported to induce up-regulation of both the B1R and B2R in murine airways (47). To investigate whether cytokine treatment with IL-1 $\beta$  and IFN- $\gamma$  increased B2R expression, we measured B1R and B2R mRNA levels in control and cytokine-treated HLMVEC using quantitative real-time RT-PCR. Consistent with our previous studies (21,44), cytokine treatment increased B1R mRNA expression (control cells B1R/GAPDH =  $0.72 \pm 0.088$ ; cytokine-treated cells B1R/GAPDH =  $1.17 \pm 0.023$ ; n = 3). However, B2R mRNA did not change after cytokine treatment (control cells B2R/GAPDH =  $1.18 \pm 0.008$ ; cytokine-treated cells B2R/GAPDH =  $1.12 \pm 0.005$ ; n = 3). In addition, cytokine treatment did not alter protein expression of  $\text{G}\alpha_{q11}$  or  $\text{G}\alpha_{i1,2}$  (data not shown).

*B2R-mediated NO production is regulated by a MEK1/2 and JNK1/2- dependent pathway in cytokine-treated endothelial cells* - We previously showed that B1R-dependent activation of prolonged NO output via iNOS in cytokine-treated HLMVEC is dependent on activation of the MEK1/2 – ERK1/2 MAP kinase pathway (11-13). Because B2R stimulation has been reported to activate ERK (16,48), we evaluated the role of this pathway in B2R-mediated NO production in control and cytokine-treated HLMVEC using three structurally distinct MEK1/2 inhibitors: PD98059 (25  $\mu\text{M}$ ), U0126 (10  $\mu\text{M}$ ) and CI-1040 (2  $\mu\text{M}$ ).

As shown in Fig. 7A, all 3 inhibitors significantly reduced B2R-mediated NO production from cytokine-treated HLMVEC, but had little effect in control endothelial cells. The negative control compound, U0124 (10  $\mu\text{M}$ ), a structurally similar but inactive analogue of U0126, did not alter B2R-mediated NO production in control or cytokine-treated HLMVEC. MEK1/2 inhibitors also significantly blocked the prolonged NO production stimulated by BK in cytokine-treated HEK-B2R/eNOS (Fig. 4B) or the B2R agonist analog,  $[\text{Phe}^8\psi(\text{CH}_2\text{-NH})\text{Arg}^9]$ bradykinin, in cytokine-treated HLMVEC (Fig. 4C).

MEK1/2 is the dual specificity kinase directly upstream of ERK1/2 activation and blockade of a signal by MEK1/2 inhibition is usually taken as prima facie evidence that the response requires activation of ERK1/2. To determine whether ERK1/2 was involved in the regulation of eNOS, we measured B2R-stimulated NO production in control and cytokine-treated HLMVEC pre-incubated in the absence or presence of a direct ERK1/2 inhibitor (FR180204; 50  $\mu\text{M}$ ) or a structurally similar inactive analogue (FR180289; 50  $\mu\text{M}$ ). Surprisingly, FR180204 did not significantly inhibit B2R-mediated NO production in either control or cytokine-treated HLMVEC compared with cells pretreated with the negative control FR180289 (Fig. 7B). As a positive control to demonstrate the effectiveness of the ERK1/2 inhibitor in these cells, we measured NO production in cytokine-treated HLMVEC in response to B1R agonist DAKD. We previously showed that B1R stimulation of high output NO results from ERK1/2-dependent phosphorylation of iNOS at Ser<sup>745</sup> leading to its acute activation (11-13). As shown in Fig. 7C, FR180204 effectively attenuated B1R-mediated NO production in cytokine-treated HLMVEC. These data support the conclusion that B2R stimulation activates eNOS via a MEK1/2-dependent but ERK1/2-independent pathway.

ERK1/2 is a relatively specific substrate of MEK1/2, but it has been reported that MEK1/2 can also phosphorylate c-Jun-N-terminal kinase (JNK) (49). To determine whether JNK1/2 was involved in the regulation of eNOS, we utilized two specific JNK1/2 inhibitors; JNK inhibitor II (SP600125; 20  $\mu\text{M}$ ) and JNK Inhibitor VIII (10  $\mu\text{M}$ ). As shown in Fig. 7D, B2R-mediated NO

production was significantly reduced in cytokine-treated HLMVEC pretreated with JNK inhibitor II or JNK Inhibitor VIII. Furthermore, knockdown of JNK1/2 expression by electroporating HLMVEC with JNK1/2 siRNA significantly reduced B2R-mediated NO production in cytokine-treated endothelial cells (Fig. 7E). In contrast, JNK1/2 siRNA had no significant effect on B2R-mediated NO production in control HLMVEC (Fig. 7F).

To determine the effect of cytokine treatment on B2R-mediated JNK1/2 activation in HLMVEC, we measured the time course of JNK1/2 phosphorylation in response to BK. We found that JNK1/2 phosphorylation increased at 1 min, reaching a maximum 3.3 - fold increase at 5 min and slowly decreasing thereafter, but still remaining elevated over basal at 30 and 60 min (Fig. 8A). In contrast, there was minimal change in JNK1/2 phosphorylation in response to BK in control HLMVEC (Fig. 8A). The activation of JNK1/2 in cytokine-treated HLMVEC required coupling through  $G\alpha_{i/o}$  as it was inhibited in cells pre-incubated with PTx (1.5  $\mu$ g/ml; 3 h) (Fig. 8B). Furthermore, as found with the NO response, B2R - mediated JNK1/2 activation in cytokine-treated HLMVEC was blocked by the MEK1/2 inhibitor U0126 (Fig. 8C) and was also reduced in cells in which MEK1/2 was knocked down with siRNA (Fig. 8D).

Because the B2R can transactivate the epidermal growth factor receptor (EGFR) (48,50), we measured NO production from cytokine-treated HLMVEC pretreated in the absence or presence of the EGFR tyrosine kinase inhibitor PD153035 (200 nM; 30 min) prior to stimulation with BK. B2R-mediated NO production was not altered by the EGFR tyrosine kinase inhibitor (data not shown). The concentration of PD153035 used was effective, as it inhibited EGF-mediated eNOS-dependent NO production and JNK phosphorylation in cytokine-treated HLMVEC (data not shown).

Overall, these data show that under inflammatory conditions, B2R stimulation induces eNOS activation and prolonged NO output by a  $G\alpha_{i/o}$ -mediated, MEK1/2 and JNK1/2-dependent pathway in HLMVEC.

*B2R-mediated eNOS phosphorylation at Ser<sup>1177</sup>, Thr<sup>495</sup>, Ser<sup>114</sup>, Ser<sup>615</sup> or Ser<sup>633</sup> does not play a role in prolonged eNOS-derived NO in cytokine-*

*treated HLMVEC* - eNOS activity is tightly regulated by a variety of mechanisms, most notably by dephosphorylation at the inhibitory site Thr<sup>495</sup> and PI3K/Akt-dependent phosphorylation at the stimulatory site Ser<sup>1177</sup> (23-26). Additionally, eNOS activity is regulated by phosphorylation at Ser<sup>615</sup>, Ser<sup>633</sup> and Ser<sup>114</sup>, depending on the cell type and stimulus utilized (26,28,29,51,52). We investigated B2R-mediated phosphorylation of eNOS at Ser<sup>1177</sup>, Thr<sup>495</sup>, Ser<sup>615</sup>, Ser<sup>633</sup> and Ser<sup>114</sup> in cytokine-treated HLMVEC. As shown in Fig. 9A & 9B, maximum phosphorylation was observed 5 min post-BK stimulation at Ser<sup>1177</sup>, Thr<sup>495</sup> and Ser<sup>114</sup> but no significant phosphorylation was detected at Ser<sup>615</sup> or Ser<sup>633</sup>. Phosphorylation at Ser<sup>1177</sup> or Thr<sup>495</sup> returned to baseline within 15 or 30 min of receptor activation, whereas phosphorylation at Ser<sup>114</sup> declined but remained significantly elevated above baseline 30 min post-BK stimulation. To determine if JNK has a role in B2R-mediated eNOS phosphorylation at the aforementioned sites, we pre-incubated cytokine-treated HLMVEC with JNK inhibitor II (SP600125; 20  $\mu$ M) and analyzed BK-dependent phosphorylation. As shown in Figs. 9C & 9D, B2R-mediated phosphorylation at Ser<sup>1177</sup> and Ser<sup>114</sup> was not significantly inhibited by JNK inhibitor II, at a concentration that inhibited NO production (Fig. 7D). Conversely, phosphorylation of these residues in response to BK was essentially abolished in the presence of BAPTA-AM (Fig. 9C and 9D), which had no effect on prolonged NO production (Fig. 5A).

*Bradykinin has divergent effects on endothelial wound healing in control and cytokine-treated endothelial cells* - Endothelial NO production is known to regulate wound healing and angiogenesis (53,54). To determine if B2R-mediated NO production affects endothelial cell migration, we utilized the *in vitro* scratch assay (Fig. 10) and a modified Boyden Chamber assay (Fig. 11). Stimulation of control HLMVEC with BK significantly improved wound healing and increased their transmigration (Figs. 10 & 11). However, BK stimulation of cytokine-treated HLMVEC delayed wound healing and reduced transmigration of cells (Figs. 10 & 11). Furthermore, the changes in wound healing and transmigration in response to BK were mediated by B2R activation and were eNOS-dependent as both the stimulatory response in control cells and

the inhibitory response in cytokine-treated cells were blocked by B2R antagonist HOE-140 or eNOS inhibitor L-NNA. As a reduction in wound healing can also be caused by increased apoptosis, we utilized fluorescein-dUTP to label DNA at strand breaks as a marker of apoptosis. We found that B2R-mediated eNOS activation in cytokine-treated HLMVEC did not induce endothelial cell apoptosis (Fig. 10C).

NO itself enhances wound healing and angiogenesis (55), but enhanced levels of oxidative and nitroxidative stress can alter the progression of wound healing (54). To determine whether the presence of reactive oxygen species (ROS) reduces B2R-mediated NO bioavailability, we pre-incubated control and cytokine-treated HLMVEC without or with the superoxide scavengers tempol (10  $\mu$ M) or polyethylene glycol-superoxide dismutase (PEG-SOD; 100 U/ml), 30 min prior to stimulation with 1  $\mu$ M BK. We found that B2R-mediated NO production was increased by ~30% in the presence of tempol (Fig. 12A; *middle*) or PEG-SOD (Fig. 12B) in cytokine-treated HLMVEC but had no effect in control cells (Fig. 12A; *left*). Moreover, the reduction in wound healing mediated by B2R stimulation in cytokine-treated HLMVEC was inhibited in the presence of tempol (Fig. 12C & 12D). Overall, these data suggest that the presence of superoxide in inflamed endothelium reduces B2R-mediated NO bioavailability and explains part of the reduction in endothelial cell migration.

These data indicate that superoxide is generated in cytokine-treated cells and can reduce the NO detected by the microsensor. Although these results would argue against the likelihood that BK stimulation reduces superoxide-mediate consumption of NO, we assessed the maximal increase in basal NO that could be achieved by scavenging superoxide. In cytokine-treated HLMVEC (pre-treated with 1400W to block iNOS activity), addition of 100  $\mu$ M tempol generated only a small increase in detectable basal NO that returned to baseline before 20 min (Fig. 12A, right panel). These results are consistent with our finding that eNOS is basally active in cytokine-treated endothelial cells (Fig. 6B), some of which is consumed by superoxide, and that the prolonged increase in NO after B2R stimulation does not arise from blocking the consumption of basally

generated NO, but rather an increase in eNOS-derived NO production.

## DISCUSSION

iNOS is considered to be the primary source of “high output” NO in inflammation (3,19,56). This view arose from work done in rodent cells, where iNOS expression can be induced to high levels and from the fact that iNOS has basal activity that is not dependent on increased  $[Ca^{2+}]_i$  (3,19,56). Our study challenges this notion, as we find that eNOS can generate “high output” NO in human endothelium under inflammatory conditions. We found a similar response in cytokine-treated HEK cells co-transfected with eNOS and B2R. Furthermore, this response is “iNOS-like” in that eNOS has higher basal affinity for  $Ca^{2+}$ -CaM which is reflected in a higher constitutive activity and lack of a requirement for an increase in  $[Ca^{2+}]_i$  for agonist-stimulated activity (Fig. 13A). Instead, B2R-dependent eNOS activation is mediated by a novel  $G\alpha_{i/o}$ - and MEK1/2  $\rightarrow$  JNK1/2- dependent pathway in cytokine-treated HLMVEC (Fig. 13B). The ability to generate high output eNOS-derived NO is likely more relevant in humans than in rodents because iNOS expression is highly induced in rodent cells in response to LPS or cytokines but in human cells, iNOS expression is much lower and in many cases difficult to detect (3,57) due to epigenetic silencing (58). As a result, basal iNOS-derived NO is much lower in human than in rodent cells, and high output eNOS-derived NO has the potential to play a more important role in human tissues.

Electrode-based measurements of NO have the advantage of detecting real time output of authentic NO with high sensitivity. However, as this method measures changes in NO concentration, it would not distinguish between a B2R and eNOS-dependent reduction in consumption of basally generated NO and increased NO production by eNOS. Cellular NO has a relatively short half-life (< 2 sec) as it is rapidly consumed by heme-containing molecules, oxidation, nitration, nitrosation, peroxidases as well as other mechanisms, some still undefined (38,59). A major pathway for cellular consumption of NO, especially under inflammatory conditions, is the extremely rapid rate of reaction with superoxide (38,59,60) and it

has been concluded that only reactions as fast as this can effectively compete with rapid NO diffusion out of the cell (59) (where it would be detected by the electrode), thereby eliminating many known pathways. If B2R activation stimulates an increase in NO by decreasing superoxide production, we would expect the superoxide scavenger tempol to generate a similar response, which it did not. These data do not rule out BK-mediated inhibition of other, possibly unknown, mechanisms of NO consumption. Therefore, we used a well-established approach (37,61) to “clamp” cellular NO concentrations with the long half-life NO donor DETA-NONOate and found that BK had no effect on the NO consumption rate in cytokine-treated HLMVEC. One other mechanism by which B2R activation might increase eNOS-dependent NO is by enhancing reduction of NO<sub>2</sub><sup>-</sup> to NO. Although we showed that the NO response is eNOS-dependent, it has been reported that eNOS can act as a nitrite reductase (39). However, this is unlikely as the reported nitrite reductase activity of eNOS is present only under hypoxic and/or acidic conditions and is inhibited with 300 μM L-Arg (39) (our medium contains 400 μM L-Arg). Indeed, stimulation of cytokine-treated HLMVEC with BK in L-Arg-free medium in the presence of 10 μM NO<sub>2</sub><sup>-</sup> [which yields maximal eNOS-mediated nitrite reductase activity(39)] did not generate any NO. Finally, total NO<sub>2</sub><sup>-</sup>/ NO<sub>3</sub><sup>-</sup> accumulation was significantly increased after BK stimulation in cytokine-treated HEK-B2R/eNOS cells, but was undetectable after stimulation of control HEK-B2R/eNOS cells. Taken together, our evidence supports the conclusion that the prolonged NO output generated by B2R activation in cytokine-treated HLMVEC results from activation of eNOS.

We found that B2R-mediated eNOS activation was independent of increased [Ca<sup>2+</sup>]<sub>i</sub>. Although Ca<sup>2+</sup>-CaM binding is required for the activity of all three NOS isoforms, the “calcium-independence” of iNOS is due to its high affinity for Ca<sup>2+</sup>-CaM, which does not dissociate at normal low concentrations of [Ca<sup>2+</sup>]<sub>i</sub> (62). Interestingly, we found a ~4-fold increase in the level Ca<sup>2+</sup>-CaM pulled down with eNOS isolated from cytokine-treated HLMVEC compared with control cells. Consistent with this, we also found that L-Arg stimulates significant basal eNOS-dependent NO

production in cytokine-treated HLMVEC, but not in control cells. This may also serve as a “priming” mechanism, rendering eNOS more susceptible to prolonged activation in response to B2R stimulation. Although the mechanism of this enhanced Ca<sup>2+</sup>-CaM binding to eNOS is unknown, it could involve altering the phosphorylation state of residues in or near the Ca<sup>2+</sup>-CaM binding region. Three domains in eNOS inhibit its interaction with CaM at resting Ca<sup>2+</sup> levels: 1. an auto-inhibitory loop (a.a. 595-639) located within the FMN binding domain (63,64); 2. a C-terminal tail extension (a.a. 1165-1178) present in the reductase domain (65); 3. a highly conserved loop (CD2A) within the connecting domain (66). Phosphorylation at several sites on eNOS can increase its sensitivity to [Ca<sup>2+</sup>]<sub>i</sub>; most likely through disruption of one or more of the control elements (e.g., phosphorylation at Ser<sup>1177</sup>, Ser<sup>633</sup>, Ser<sup>615</sup>) or removal of direct repulsion of Ca<sup>2+</sup>-CaM binding by dephosphorylation of p-Thr<sup>495</sup> (24). Thus, cytokine treatment might activate a kinase or phosphatase that alters the phosphorylation state of one of the Ca<sup>2+</sup>-CaM control elements. While our data regarding basal eNOS phosphorylation at the aforementioned sites do not clearly indicate a reason for enhanced Ca<sup>2+</sup>-CaM binding, it is important to emphasize that we were measuring total eNOS phosphorylation, which may not reflect differences in its phosphorylation at relevant sub-cellular sites. For example, the phosphorylation state of eNOS was shown to differ depending on its sub-cellular localization, with eNOS phosphorylated at Thr<sup>495</sup> being restricted to caveolar fractions (67). Thus, the fraction of eNOS tightly associated with Ca<sup>2+</sup>-CaM may be localized in non-caveolar fractions where Thr<sup>495</sup> is not phosphorylated, consistent with the reciprocal relationship between caveolin and Ca<sup>2+</sup>-CaM binding to eNOS (22).

JNK is classically activated by upstream kinases MKK4 and MKK7 which is typically induced by cellular stress and/or activation of Gα<sub>12/13</sub>-coupled receptors (68,69). The B2R is classified as a prototypical Gα<sub>q/11</sub> - coupled receptor but can also couple to Gα<sub>i/o</sub> (16). We found that B2R-mediated JNK1/2 phosphorylation and NO production were PTx-sensitive, showing that JNK1/2 is activated downstream of B2Rs coupled to Gα<sub>i/o</sub>, consistent previous reports that

$G\alpha_{i/o}$  and associated  $G\beta\gamma$ -subunits can activate JNK (69-71). Surprisingly, we found  $G\alpha_{i/o}$ -dependent JNK phosphorylation to be downstream of MEK1/2, although  $G\alpha_{i/o}$ -dependent JNK activation has been reported to be independent of MKK4/7 (70) and one report showed MEK1/2 to phosphorylate JNK in a human astrocyte (U-251) cell line (49).

JNKs are proline-directed Ser/Thr kinases that phosphorylate many nuclear and cytosolic substrates (72). Human eNOS contains 15 Ser/Thr residues that are potential JNK phosphorylation sites as determined using ExPASy ScanProsite. However, JNK often utilizes a docking domain (R/K<sub>2-3</sub>-X<sub>1-6</sub>-L/I-X-L/I) on the substrate or on a scaffold protein that facilitates JNK interaction with substrates lacking a JNK binding domain (JBD) (72,73), which confers enhanced specificity of phosphorylation. Although human eNOS does not contain a typical JBD, JNK might interact with a novel JBD in eNOS or with a scaffold protein containing a JBD to facilitate eNOS phosphorylation. JNK has not been linked to eNOS activation, but was recently reported to basally phosphorylate eNOS at Ser<sup>116</sup> (bovine numbering) to reduce eNOS-derived NO in bovine aortic endothelial cells (52). In contrast, we found that B2R-mediated JNK activation was required for stimulation of prolonged eNOS activity, which was independent of phosphorylation at the well-known regulatory sites. These data suggest that JNK controls eNOS activation by a different mechanism, possibly via phosphorylation at a novel regulatory site. Alternatively, JNK may activate another kinase that phosphorylates eNOS (Fig. 13B) or the activation process may be independent of eNOS phosphorylation, for example by altering protein interactions with eNOS or eNOS localization (23,74).

Enhanced B2R-mediated signaling and eNOS-dependent NO output after cytokine treatment could be facilitated by mechanisms in addition to increased  $Ca^{2+}$ -CaM binding. Cytokines alter cell functions by promoting significant changes in gene expression and protein synthesis (43). Although cytokine treatment did not alter B2R mRNA levels or the protein expression of  $G\alpha_{q/11}$ ,  $G\alpha_{i1,2}$ , eNOS or JNK, B2R-mediated JNK activation was more robust in cytokine-treated HLMVEC. However, cytokine treatment might

alter the membrane microdomain localization of signaling components without altering their overall expression. For example,  $G\alpha_{q/11}$  binds caveolin to concentrate in caveolae, whereas  $G\alpha_{i/o}$  targets lipid rafts by default (75). B2Rs and eNOS localize to caveolae in healthy endothelial cells (76), but inflammation can induce changes in membrane phospholipid composition that affects cholesterol-rich microdomains to alter signal transduction (77). Thus, it is possible that cytokine treatment promotes segregation of B2Rs into lipid raft microdomains, enhancing its  $G\alpha_{i/o}$ -dependent signaling and eNOS activation. Cytokine treatment could also alter post-translational modifications of the B2R that might facilitate  $G\alpha_{i/o}$  coupling. Alternatively, it may not be B2R- $G\alpha_{i/o}$  coupling that is enhanced by cytokines, but downstream components. For example, MAP kinases rely on scaffolding proteins to amplify and modulate the specificity of their responses (72,73). Thus, cytokine treatment might induce the expression of a scaffold protein or facilitate its binding to MEK1/2, JNK1/2 and eNOS to allow efficient activation to occur. Interestingly, although cytokine treatment enhanced signaling via  $G\alpha_{i/o}$  and JNK,  $Ca^{2+}$  signaling through  $G\alpha_{q/11}$  was also increased, indicating a major switch of B2R coupling from  $G\alpha_{q/11}$  to  $G\alpha_{i/o}$  is likely not the primary mechanism.

Endothelial-derived NO and its derivatives play critical roles in regulating normal vascular functions, but can also be involved in exacerbating or ameliorating cardiovascular diseases (8,10,56,60). For example, NO is a major regulator of angiogenesis and plays important roles in wound healing (53). We found that B2R-mediated eNOS-derived NO has opposing effects on endothelial cell migration in control and cytokine-treated HLMVEC, promoting migration in control cells but inhibiting migration in cytokine-treated endothelial cells. Thus, prolonged B2R-mediated NO production might reduce angiogenesis as it was recently shown that caveolin1-deficient mice have impaired angiogenesis which is partially mediated by increased eNOS activation (78). The mechanism by which NO regulates endothelial cell migration is not understood, but VEGF-induced angiogenesis is dependent on NO production and subsequent increased cGMP and PKG activation, resulting in

phosphorylation and activation of p38 and ERK1/2 (79). While NO clearly plays a pro-migratory role, the balance between the concentration of NO and level of oxidative and nitroxidative stress can differentially regulate its effect on the endothelium (54). For example, although NO itself is pro-migratory, under inflammatory conditions, combined with superoxide to generate ONOO<sup>-</sup>, it could inhibit migration (54). This is consistent with our finding that scavenging of superoxide with tempol or PEG-SOD enhanced the NO detected in response to BK in cytokine-treated HLMVEC and reduced the inhibition of cell migration. However, it is interesting that in the presence of tempol, BK did not stimulate cell migration it did in control HLMVEC. This could be due to the higher and more prolonged output of NO generated under inflammatory conditions.

HLMVEC in the lung circulation form the essential semi-permeable barrier that dynamically regulates the passage of fluid and protein (80). Sepsis is a leading cause of acute lung injury characterized by inflammation and increased lung microvascular endothelial permeability. The precise role of NO in sepsis and lung inflammation is still controversial. Studies have shown that NO production may have both salutary and harmful effects. A general theme is that low output NO promotes barrier function whereas high output NO, especially when combined with oxidants, is damaging and increases permeability (9,14,81,82). For example, caveolin-1 depletion results in microvascular hyperpermeability, which may be due to increased eNOS-derived NO (82,83), whereas decreased NO production caused by eNOS gene deletion or NOS inhibition also increased vascular permeability(84). Thus, a proper range of NO concentration is crucial in maintaining endothelial barrier function. NO regulates vascular permeability via activation of guanylate cyclase (85) or nitrosylation of cysteine residues on critical signaling molecules. For example, VEGF-mediated eNOS activation induces nitrosylation of  $\beta$ -catenin, thereby

disrupting its association with VE-cadherin and increasing endothelial permeability via the paracellular pathway (86). VEGF also enhances endothelial permeability by stimulating  $\beta$ -catenin endocytosis that is dependent on  $\beta$ -arrestin 2 (87) and S-nitrosylation of  $\beta$ -arrestin 2 promotes its binding to clathrin heavy chain/beta-adaptin, thereby inducing endocytosis (88). Under inflammatory conditions, ONOO<sup>-</sup> generation becomes an important mediator of enhanced endothelial permeability. ONOO<sup>-</sup>, via Tyr nitration, activates protein phosphatase 2A (89) or inactivates actin (90) or p190RhoGAP-A (91) and as an oxidant it activates tyrosine kinases such as Src or inactivates phosphatases such as PTP1B (60), all of which can disrupt the endothelial barrier.

Overall, the findings of this study blur the traditional distinctions between the functions of eNOS and iNOS in generating NO in inflammation. Furthermore, our previous studies have challenged the view that iNOS is only regulated at the level of expression or substrate supply, functioning as a constitutively active, uncontrolled generator of NO (1,3,56). That is, the control of iNOS activity is more complex and “eNOS-like” than previously recognized. We found that stimulation of the kinin B1R in cytokine-treated HLMVEC or transfected HEK cells results in signaling through a  $G\alpha_{i/o}$ -,  $\beta\gamma$ - and  $\beta$ -arrestin 2- dependent pathway activating Src $\rightarrow$ Ras $\rightarrow$ Raf $\rightarrow$ MEK1/2 $\rightarrow$ ERK1/2 (11-13). ERK1/2 in turn phosphorylates iNOS at Ser<sup>745</sup>, leading to a 3- to 5-fold increase in iNOS activity over basal (11). The presence of both eNOS and iNOS-dependent high output NO pathways in inflamed endothelium could have important consequences in regulating endothelial function and a better understanding of their roles could lead to new therapeutic approaches to ameliorate endothelial dysfunction caused by overproduction of NO in inflammatory vascular or lung disease.

## REFERENCES

1. Alderton, W. K., Cooper, C. E., and Knowles, R. G. Nitric oxide synthases: structure, function and inhibition. (2001) *Biochem. J.* **357**, 593-615
2. Aktan, F. iNOS-mediated nitric oxide production and its regulation. (2004) *Life Sci.* **75**, 639-653
3. Kleinert, H., Pautz, A., Linker, K., and Schwarz, P. M. Regulation of the expression of inducible nitric oxide synthase. (2004) *Eur. J. Pharmacol.* **500**, 255-266
4. Villanueva, C., and Giulivi, C. Subcellular and cellular locations of nitric oxide synthase isoforms as determinants of health and disease. (2010) *Free Radic. Biol. Med.* **49**, 307-316
5. Hill, B. G., Dranka, B. P., Bailey, S. M., Lancaster, J. R., Jr., and Darley-Usmar, V. M. What part of NO don't you understand? Some answers to the cardinal questions in nitric oxide biology. (2010) *J. Biol. Chem.* **285**, 19699-19704
6. Albrecht, E. W., Stegeman, C. A., Heeringa, P., Henning, R. H., and van Goor, H. Protective role of endothelial nitric oxide synthase. (2003) *J. Pathol.* **199**, 8-17
7. Cooke, J. P., and Dzau, V. J. Derangements of the nitric oxide synthase pathway, L-arginine, and cardiovascular diseases. (1997) *Circulation* **96**, 379-382
8. Beckman, J. S., and Koppenol, W. H. Nitric oxide, superoxide, and peroxynitrite: the good, the bad, and ugly. (1996) *Am. J. Physiol.* **271**, C1424-1437
9. Zamora, R., Vodovotz, Y., and Billiar, T. R. Inducible nitric oxide synthase and inflammatory diseases. (2000) *Mol. Med.* **6**, 347-373
10. Chatterjee, A., Black, S. M., and Catravas, J. D. Endothelial nitric oxide (NO) and its pathophysiologic regulation. (2008) *Vascul. Pharmacol.* **49**, 134-140
11. Zhang, Y., Brovkovych, V., Brovkovych, S., Tan, F., Lee, B. S., Sharma, T., and Skidgel, R. A. Dynamic receptor-dependent activation of inducible nitric-oxide synthase by ERK-mediated phosphorylation of Ser745. (2007) *J. Biol. Chem.* **282**, 32453-32461
12. Brovkovych, V., Zhang, Y., Brovkovych, S., Minshall, R. D., and Skidgel, R. A. A novel pathway for receptor-mediated post-translational activation of inducible nitric oxide synthase. (2011) *J. Cell. Mol. Med.* **15**, 258-269
13. Kuhr, F. K., Zhang, Y., Brovkovych, V., and Skidgel, R. A.  $\beta$ -Arrestin 2 is required for B1 receptor-dependent post-translational activation of inducible nitric oxide synthase. (2010) *FASEB J.* **24**, 2475-2483
14. Cirino, G., Fiorucci, S., and Sessa, W. C. Endothelial nitric oxide synthase: the Cinderella of inflammation? (2003) *Trends Pharmacol. Sci.* **24**, 91-95
15. Bhoola, K. D., Figueroa, C. D., and Worthy, K. Bioregulation of kinins: kallikreins, kininogens, and kininases. (1992) *Pharmacol. Rev.* **44**, 1-80
16. Leeb-Lundberg, L. M., Marceau, F., Muller-Esterl, W., Pettibone, D. J., and Zuraw, B. L. International union of pharmacology. XLV. Classification of the kinin receptor family: from molecular mechanisms to pathophysiological consequences. (2005) *Pharmacol. Rev.* **57**, 27-77
17. Zhang, X., Tan, F., Brovkovych, V., Zhang, Y., and Skidgel, R. A. Cross-talk between carboxypeptidase M and the kinin B1 receptor mediates a new mode of G protein-coupled receptor signaling. (2011) *J. Biol. Chem.* **286**, 18547-18561
18. Zhang, X., Tan, F., Zhang, Y., and Skidgel, R. A. Carboxypeptidase M and kinin B1 receptors interact to facilitate efficient b1 signaling from B2 agonists. (2008) *J. Biol. Chem.* **283**, 7994-8004
19. Kuhr, F., Lowry, J., Zhang, Y., Brovkovych, V., and Skidgel, R. A. Differential regulation of inducible and endothelial nitric oxide synthase by kinin B1 and B2 receptors. (2010) *Neuropeptides* **44**, 145-154
20. Venema, R. C. Post-translational mechanisms of endothelial nitric oxide synthase regulation by bradykinin. (2002) *Int. Immunopharmacol.* **2**, 1755-1762

21. Sangsree, S., Brovkovich, V., Minshall, R. D., and Skidgel, R. A. Kininase I-type carboxypeptidases enhance nitric oxide production in endothelial cells by generating bradykinin B1 receptor agonists. (2003) *Am. J. Physiol. Heart Circ. Physiology* **284**, H1959-1968
22. Fulton, D., Gratton, J. P., and Sessa, W. C. Post-translational control of endothelial nitric oxide synthase: why isn't calcium/calmodulin enough? (2001) *J. Pharmacol. Exp. Ther.* **299**, 818-824
23. Dudzinski, D. M., and Michel, T. Life history of eNOS: partners and pathways. (2007) *Cardiovasc. Res.* **75**, 247-260
24. Rafikov, R., Fonseca, F. V., Kumar, S., Pardo, D., Darragh, C., Elms, S., Fulton, D., and Black, S. M. eNOS activation and NO function: structural motifs responsible for the posttranslational control of endothelial nitric oxide synthase activity. (2011) *J. Endocrinol.* **210**, 271-284
25. Harris, M. B., Ju, H., Venema, V. J., Liang, H., Zou, R., Michell, B. J., Chen, Z. P., Kemp, B. E., and Venema, R. C. Reciprocal phosphorylation and regulation of endothelial nitric-oxide synthase in response to bradykinin stimulation. (2001) *J. Biol. Chem.* **276**, 16587-16591
26. Fleming, I. Molecular mechanisms underlying the activation of eNOS. (2010) *Pflugers Arch.* **459**, 793-806
27. Fulton, D., Ruan, L., Sood, S. G., Li, C., Zhang, Q., and Venema, R. C. Agonist-stimulated endothelial nitric oxide synthase activation and vascular relaxation. Role of eNOS phosphorylation at Tyr83. (2008) *Circ. Res.* **102**, 497-504
28. Michell, B. J., Harris, M. B., Chen, Z. P., Ju, H., Venema, V. J., Blackstone, M. A., Huang, W., Venema, R. C., and Kemp, B. E. Identification of regulatory sites of phosphorylation of the bovine endothelial nitric-oxide synthase at serine 617 and serine 635. (2002) *J. Biol. Chem.* **277**, 42344-42351
29. Xiao, Z., Wang, T., Qin, H., Huang, C., Feng, Y., and Xia, Y. Endoplasmic reticulum Ca<sup>2+</sup> release modulates endothelial nitric-oxide synthase via extracellular signal-regulated kinase (ERK) 1/2-mediated serine 635 phosphorylation. (2011) *J. Biol. Chem.* **286**, 20100-20108
30. Casanello, P., Krause, B., Torres, E., Gallardo, V., Gonzalez, M., Prieto, C., Escudero, C., Farias, M., and Sobrevia, L. Reduced l-arginine transport and nitric oxide synthesis in human umbilical vein endothelial cells from intrauterine growth restriction pregnancies is not further altered by hypoxia. (2009) *Placenta* **30**, 625-633
31. Ussar, S., and Voss, T. MEK1 and MEK2, different regulators of the G1/S transition. (2004) *J. Biol. Chem.* **279**, 43861-43869
32. Gross, N. D., Boyle, J. O., Du, B., Kekatpure, V. D., Lantowski, A., Thaler, H. T., Weksler, B. B., Subbaramaiah, K., and Dannenberg, A. J. Inhibition of Jun NH2-terminal kinases suppresses the growth of experimental head and neck squamous cell carcinoma. (2007) *Clin. Cancer Res.* **13**, 5910-5917
33. Brovkovich, V., Stolarczyk, E., Oman, J., Tomboulian, P., and Malinski, T. Direct electrochemical measurement of nitric oxide in vascular endothelium. (1999) *J. Pharm. Biomed. Anal.* **19**, 135-143
34. Liesmaa, I., Leskinen, H. K., Kokkonen, J. O., Ruskoaho, H., Kovanen, P. T., and Lindstedt, K. A. Hypoxia-induced expression of bradykinin type-2 receptors in endothelial cells triggers NO production, cell migration, and angiogenesis. (2009) *J. Cell. Physiol.* **221**, 359-366
35. Liang, C. C., Park, A. Y., and Guan, J. L. In vitro scratch assay: a convenient and inexpensive method for analysis of cell migration in vitro. (2007) *Nat. Protoc.* **2**, 329-333
36. Drapeau, G., Rhaleb, N. E., Dion, S., Jukic, D., and Regoli, D. [Phe<sup>8</sup> psi(CH<sub>2</sub>-NH)Arg<sup>9</sup>]bradykinin, a B2 receptor selective agonist which is not broken down by either kininase I or kininase II. (1988) *Eur. J. Pharmacol.* **155**, 193-195
37. Griffiths, C., and Garthwaite, J. The shaping of nitric oxide signals by a cellular sink. (2001) *J. Physiol.* **536**, 855-862
38. Thomas, D. D., Ridnour, L. A., Isenberg, J. S., Flores-Santana, W., Switzer, C. H., Donzelli, S., Hussain, P., Vecoli, C., Paolocci, N., Ambs, S., Colton, C. A., Harris, C. C., Roberts, D. D., and

- Wink, D. A. The chemical biology of nitric oxide: implications in cellular signaling. (2008) *Free Radic. Biol. Med.* **45**, 18-31
39. Webb, A. J., Milsom, A. B., Rathod, K. S., Chu, W. L., Qureshi, S., Lovell, M. J., Lecomte, F. M., Perrett, D., Raimondo, C., Khoshbin, E., Ahmed, Z., Uppal, R., Benjamin, N., Hobbs, A. J., and Ahluwalia, A. Mechanisms underlying erythrocyte and endothelial nitrite reduction to nitric oxide in hypoxia: role for xanthine oxidoreductase and endothelial nitric oxide synthase. (2008) *Circ. Res.* **103**, 957-964
40. Closs, E. I. Expression, regulation and function of carrier proteins for cationic amino acids. (2002) *Curr. Opin. Nephrol. Hypertens.* **11**, 99-107
41. Luhrs, H., Papadopoulos, T., Schmidt, H. H., and Menzel, T. Type I nitric oxide synthase in the human lung is predominantly expressed in capillary endothelial cells. (2002) *Respir. Physiol.* **129**, 367-374
42. Bachetti, T., Comini, L., Curello, S., Bastianon, D., Palmieri, M., Bresciani, G., Callea, F., and Ferrari, R. Co-expression and modulation of neuronal and endothelial nitric oxide synthase in human endothelial cells. (2004) *J. Mol. Cell. Cardiol.* **37**, 939-945
43. Mantovani, A., Bussolino, F., and Dejana, E. Cytokine regulation of endothelial cell function. (1992) *FASEB J.* **6**, 2591-2599
44. Ignjatovic, T., Stanisavljevic, S., Brovkovich, V., Skidgel, R. A., and Erdos, E. G. Kinin B1 receptors stimulate nitric oxide production in endothelial cells: signaling pathways activated by angiotensin I-converting enzyme inhibitors and peptide ligands. (2004) *Mol. Pharmacol.* **66**, 1310-1316
45. Zimmerman, B., Simaan, M., Akoume, M. Y., Hourri, N., Chevallier, S., Seguela, P., and Laporte, S. A. Role of  $\beta$  arrestins in bradykinin B2 receptor-mediated signalling (2011) *Cell. Signal.* **23**, 648-659
46. Closs, E. I., Scheld, J. S., Sharafi, M., and Forstermann, U. Substrate supply for nitric-oxide synthase in macrophages and endothelial cells: role of cationic amino acid transporters. (2000) *Mol. Pharmacol.* **57**, 68-74
47. Zhang, Y., Adner, M., and Cardell, L. O. IL-1 $\beta$ -induced transcriptional up-regulation of bradykinin B1 and B2 receptors in murine airways. (2007) *Am. J. Respir. Cell Mol. Biol.* **36**, 697-705
48. Blaukat, A., Barac, A., Cross, M. J., Offermanns, S., and Dikic, I. G protein-coupled receptor-mediated mitogen-activated protein kinase activation through cooperation of Galpha(q) and Galpha(i) signals. (2000) *Mol. Cell. Biol.* **20**, 6837-6848
49. Adler, V., Qu, Y., Smith, S. J., Izotova, L., Pestka, S., Kung, H. F., Lin, M., Friedman, F. K., Chie, L., Chung, D., Boutjdir, M., and Pincus, M. R. Functional interactions of Raf and MEK with Jun-N-terminal kinase (JNK) result in a positive feedback loop on the oncogenic Ras signaling pathway. (2005) *Biochemistry (Mosc).* **44**, 10784-10795
50. Adomeit, A., Graness, A., Gross, S., Seedorf, K., Wetzker, R., and Liebmann, C. Bradykinin B(2) receptor-mediated mitogen-activated protein kinase activation in COS-7 cells requires dual signaling via both protein kinase C pathway and epidermal growth factor receptor transactivation. (1999) *Mol. Cell. Biol.* **19**, 5289-5297
51. Ruan, L., Torres, C. M., Qian, J., Chen, F., Mintz, J. D., Stepp, D. W., Fulton, D., and Venema, R. C. Pin1 prolyl isomerase regulates endothelial nitric oxide synthase. (2011) *Arterioscler. Thromb. Vasc. Biol.* **31**, 392-398
52. Park, J. H., Park, M., Byun, C. J., and Jo, I. c-Jun N-terminal kinase 2 phosphorylates endothelial nitric oxide synthase at serine 116 and regulates nitric oxide production. (2012) *Biochem. Biophys. Res. Commun.* **417**, 340-345
53. Lamallice, L., Le Boeuf, F., and Huot, J. Endothelial cell migration during angiogenesis. (2007) *Circ. Res.* **100**, 782-794
54. Soneja, A., Drews, M., and Malinski, T. Role of nitric oxide, nitroxidative and oxidative stress in wound healing. (2005) *Pharmacol. Rep.* **57 Suppl**, 108-119

55. Lee, P. C., Salyapongse, A. N., Bragdon, G. A., Shears, L. L., 2nd, Watkins, S. C., Edington, H. D., and Billiar, T. R. Impaired wound healing and angiogenesis in eNOS-deficient mice. (1999) *Am. J. Physiol.* **277**, H1600-1608
56. Papapetropoulos, A., Rudic, R. D., and Sessa, W. C. Molecular control of nitric oxide synthases in the cardiovascular system. (1999) *Cardiovasc. Res.* **43**, 509-520
57. MacMicking, J., Xie, Q.-w., and Nathan, C. Nitric oxide and macrophage function. (1997) *Annu. Rev. Immunol.* **15**, 323-350
58. Chan, G. C., Fish, J. E., Mawji, I. A., Leung, D. D., Rachlis, A. C., and Marsden, P. A. Epigenetic basis for the transcriptional hyporesponsiveness of the human inducible nitric oxide synthase gene in vascular endothelial cells. (2005) *J. Immunol.* **175**, 3846-3861
59. Lancaster, J. R., Jr. Nitroxidative, nitrosative, and nitrative stress: kinetic predictions of reactive nitrogen species chemistry under biological conditions. (2006) *Chem. Res. Toxicol.* **19**, 1160-1174
60. Pacher, P., Beckman, J. S., and Liaudet, L. Nitric oxide and peroxynitrite in health and disease. (2007) *Physiol. Rev.* **87**, 315-424
61. Bellamy, T. C., Griffiths, C., and Garthwaite, J. Differential sensitivity of guanylyl cyclase and mitochondrial respiration to nitric oxide measured using clamped concentrations. (2002) *J. Biol. Chem.* **277**, 31801-31807
62. Cho, H., Xie, Q., Calaycay, J., Mumford, R., Swiderek, K., Lee, T., and Nathan, C. Calmodulin is a subunit of nitric oxide synthase from macrophages. (1992) *J. Exp. Med.* **176**, 599-604
63. Nishida, C. R., and Ortiz de Montellano, P. R. Autoinhibition of endothelial nitric-oxide synthase. Identification of an electron transfer control element. (1999) *J. Biol. Chem.* **274**, 14692-14698
64. Salerno, J. C., Harris, D. E., Irizarry, K., Patel, B., Morales, A. J., Smith, S. M., Martasek, P., Roman, L. J., Masters, B. S., Jones, C. L., Weissman, B. A., Lane, P., Liu, Q., and Gross, S. S. An autoinhibitory control element defines calcium-regulated isoforms of nitric oxide synthase. (1997) *J. Biol. Chem.* **272**, 29769-29777
65. Chen, P. F., and Wu, K. K. Structural elements contribute to the calcium/calmodulin dependence on enzyme activation in human endothelial nitric-oxide synthase. (2003) *J. Biol. Chem.* **278**, 52392-52400
66. Knudsen, G. M., Nishida, C. R., Mooney, S. D., and Ortiz de Montellano, P. R. Nitric-oxide synthase (NOS) reductase domain models suggest a new control element in endothelial NOS that attenuates calmodulin-dependent activity. (2003) *J. Biol. Chem.* **278**, 31814-31824
67. Ramadoss, J., Liao, W. X., Morschauser, T. J., Lopez, G. E., Patankar, M. S., Chen, D. B., and Magness, R. R. Endothelial caveolar hub regulation of adenosine triphosphate-induced endothelial nitric oxide synthase subcellular partitioning and domain-specific phosphorylation. (2012) *Hypertension* **59**, 1052-1059
68. Haeusgen, W., Herdegen, T., and Waetzig, V. The bottleneck of JNK signaling: molecular and functional characteristics of MKK4 and MKK7. (2011) *Eur. J. Cell Biol.* **90**, 536-544
69. Goldsmith, Z. G., and Dhanasekaran, D. N. G protein regulation of MAPK networks. (2007) *Oncogene* **26**, 3122-3142
70. Yamauchi, J., Kawano, T., Nagao, M., Kaziro, Y., and Itoh, H. G(i)-dependent activation of c-Jun N-terminal kinase in human embryonal kidney 293 cells. (2000) *J. Biol. Chem.* **275**, 7633-7640
71. Coso, O. A., Teramoto, H., Simonds, W. F., and Gutkind, J. S. Signaling from G protein-coupled receptors to c-Jun kinase involves beta gamma subunits of heterotrimeric G proteins acting on a Ras and Rac1-dependent pathway. (1996) *J. Biol. Chem.* **271**, 3963-3966
72. Bogoyevitch, M. A., and Kobe, B. Uses for JNK: the many and varied substrates of the c-Jun N-terminal kinases. (2006) *Microbiol. Mol. Biol. Rev.* **70**, 1061-1095
73. Engstrom, W., Ward, A., and Moorwood, K. The role of scaffold proteins in JNK signalling. (2010) *Cell Prolif.* **43**, 56-66
74. Skidgel, R. A. Proliferation of regulatory mechanisms for eNOS: an emerging role for the cytoskeleton. (2002) *Am. J. Physiol. Lung Cell Mol. Physiol.* **282**, L1179-1182

75. Oh, P., and Schnitzer, J. E. Segregation of heterotrimeric G proteins in cell surface microdomains. G(q) binds caveolin to concentrate in caveolae, whereas G(i) and G(s) target lipid rafts by default. (2001) *Mol. Biol. Cell* **12**, 685-698
76. Solomonson, L. P., Flam, B. R., Pendleton, L. C., Goodwin, B. L., and Eichler, D. C. The caveolar nitric oxide synthase/arginine regeneration system for NO production in endothelial cells. (2003) *J. Exp. Biol.* **206**, 2083-2087
77. Fessler, M. B., and Parks, J. S. Intracellular lipid flux and membrane microdomains as organizing principles in inflammatory cell signaling. (2011) *J. Immunol.* **187**, 1529-1535
78. Morais, C., Ebrahim, Q., Anand-Apte, B., and Parat, M. O. Altered Angiogenesis in Caveolin-1 Gene-Deficient Mice Is Restored by Ablation of Endothelial Nitric Oxide Synthase. (2012) *Am. J. Pathol.*
79. Koika, V., Zhou, Z., Vasileiadis, I., Roussos, C., Finetti, F., Monti, M., Morbidelli, L., and Papapetropoulos, A. PKG-I inhibition attenuates vascular endothelial growth factor-stimulated angiogenesis. (2010) *Vascul. Pharmacol.* **53**, 215-222
80. Mehta, D., and Malik, A. B. Signaling mechanisms regulating endothelial permeability. (2006) *Physiol. Rev.* **86**, 279-367
81. Kubes, P. Nitric oxide affects microvascular permeability in the intact and inflamed vasculature. (1995) *Microcirculation* **2**, 235-244
82. Schubert, W., Frank, P. G., Woodman, S. E., Hyogo, H., Cohen, D. E., Chow, C. W., and Lisanti, M. P. Microvascular hyperpermeability in caveolin-1 (-/-) knock-out mice. Treatment with a specific nitric-oxide synthase inhibitor, L-NAME, restores normal microvascular permeability in Cav-1 null mice. (2002) *J. Biol. Chem.* **277**, 40091-40098
83. Miyawaki-Shimizu, K., Predescu, D., Shimizu, J., Broman, M., Predescu, S., and Malik, A. B. siRNA-induced caveolin-1 knockdown in mice increases lung vascular permeability via the junctional pathway. (2006) *Am J Physiol Lung Cell Mol Physiol* **290**, L405-413
84. Predescu, D., Predescu, S., Shimizu, J., Miyawaki-Shimizu, K., and Malik, A. B. Constitutive eNOS-derived nitric oxide is a determinant of endothelial junctional integrity. (2005) *Am J Physiol Lung Cell Mol Physiol* **289**, L371-381
85. Yuan, S. Y. Signal transduction pathways in enhanced microvascular permeability. (2000) *Microcirculation* **7**, 395-403
86. Thibeault, S., Rautureau, Y., Oubaha, M., Faubert, D., Wilkes, B. C., Delisle, C., and Gratton, J. P. S-nitrosylation of beta-catenin by eNOS-derived NO promotes VEGF-induced endothelial cell permeability. (2010) *Mol Cell* **39**, 468-476
87. Gavard, J., and Gutkind, J. S. VEGF controls endothelial-cell permeability by promoting the beta-arrestin-dependent endocytosis of VE-cadherin. (2006) *Nat Cell Biol* **8**, 1223-1234
88. Ozawa, K., Whalen, E. J., Nelson, C. D., Mu, Y., Hess, D. T., Lefkowitz, R. J., and Stamler, J. S. S-nitrosylation of beta-arrestin regulates beta-adrenergic receptor trafficking. (2008) *Mol. Cell* **31**, 395-405
89. Wu, F., and Wilson, J. X. Peroxynitrite-dependent activation of protein phosphatase type 2A mediates microvascular endothelial barrier dysfunction. (2008) *Cardiovasc. Res.*
90. Neumann, P., Gertzberg, N., Vaughan, E., Weisbrot, J., Woodburn, R., Lambert, W., and Johnson, A. Peroxynitrite mediates TNF-alpha-induced endothelial barrier dysfunction and nitration of actin. (2006) *Am J Physiol Lung Cell Mol Physiol* **290**, L674-L684
91. Siddiqui, M. R., Komarova, Y. A., Vogel, S. M., Gao, X., Bonini, M. G., Rajasingh, J., Zhao, Y. Y., Brovkovich, V., and Malik, A. B. Caveolin-1-eNOS signaling promotes p190RhoGAP-A nitration and endothelial permeability. (2011) *J. Cell Biol.* **193**, 841-850

*Acknowledgments*—We thank Svitlana Brovkovich for excellent cell culture assistance.

## FOOTNOTES

\*This work was supported by the National Institutes of Health Grants PO1 HL60678, T32 HL072742 and RO1 HL36473. Jessica L. Lowry was the recipient of an American Heart Association Predoctoral Fellowship.

<sup>2</sup>To whom correspondence should be addressed: Department of Pharmacology (m/c 868), University of Illinois College of Medicine, 835 S. Wolcott, Chicago, IL 60612. Tel.: (312) 996-9179; Fax: (312) 996-1648; E-mail: rskidgel@uic.edu

<sup>3</sup>The abbreviations used are: eNOS, endothelial nitric oxide synthase; nNOS, neuronal nitric oxide synthase; iNOS, inducible nitric oxide synthase; B2R, bradykinin B2 receptor; B1R, kinin B1 receptor; BK, bradykinin; BK-analog, ([Phe<sup>8</sup>ψ(CH-NH)-Arg<sup>9</sup>]-BK; DAKD, des-Arg<sup>10</sup>-kallidin; KD, Lys<sup>10</sup>-kallidin; DALKD, des-Arg<sup>10</sup>-Leu<sup>8</sup>-kallidin; MGTA, DL-2-Mercaptomethyl-3-guanidinoethylthiopropionic acid; CP, carboxypeptidase; L-NNA, L-N<sup>G</sup>-nitro-L-arginine; BAPTA-AM, 1,2-bis(o-Aminophenoxy)ethane-N,N,N',N'-tetraacetic Acid Tetra(acetoxymethyl) Ester; PTx, pertussis toxin; 2-APB, 2-aminoethoxydiphenyl-borane; GAPDH, glyceraldehyde-3-phosphate dehydrogenase; [Ca<sup>2+</sup>]<sub>i</sub>, intracellular calcium concentration; ; HEK, human embryonic kidney; HLMVEC, human lung microvascular endothelial cell; IL-1β, interleukin-1beta; IFN-γ, interferon-gamma; MAPK, mitogen activated protein kinase; ERK, extracellular signal-regulated kinase; JNK, c-Jun N-terminal kinase; NC, negative control; EP, electroporation; siRNA, small interfering ribonucleic acid; Ca<sup>2+</sup>-CaM, calcium calmodulin; PEG-SOD, polyethylene glycol superoxide dismutase.

## FIGURE LEGENDS

**FIGURE 1.** Bradykinin (BK) and BK analog ([Phe<sup>8</sup>ψ(CH<sub>2</sub>-NH)Arg<sup>9</sup>]bradykinin) stimulates prolonged B2R-mediated, eNOS-derived NO production in cytokine-treated HLMVEC and HEK-B2R/eNOS cells. A. (*Top*) Comparison of tracings of real time measurement of BK-stimulated NO production in untreated (“control”) HLMVEC versus HLMVEC pretreated with 5 ng/mL IL-1β and 100 U/mL IFN-γ (“cytokine-treated”) for 16-24 h. (*Bottom*) B2R-mediated NO production in control and cytokine-treated HLMVEC pretreated in the absence or presence of B2R antagonist (1 μM HOE-140), eNOS selective inhibitor (4 μM L-NNA) or iNOS selective inhibitor (4 μM 1400W) 30 min prior to stimulation with 100 nM BK. B. (*Top*) Comparison of tracings of real time measurement of BK-stimulated NO production in control and cytokine-treated HEK cells transiently expressing the B2R and eNOS (HEK-B2R/eNOS). (*Bottom*) B2R-mediated NO production in control and cytokine-treated HEK-B2R/eNOS pretreated in the absence or presence of 4 μM L-NNA or 4 μM 1400W 30 min prior to stimulation with 100 nM BK. C. (*Top*) Comparison of tracings of real time measurement of BK-analog stimulated NO production in control and cytokine-treated HLMVEC. (*Bottom*) B2R-mediated NO production in control and cytokine-treated HLMVEC pretreated in the absence or presence of 10 μM HOE-140, 4 μM L-NNA or 4 μM 1400W 30 min prior to stimulation with 100 nM BK-analog. Data are expressed as mean NO concentration (% of vehicle) ± SE achieved at the peak maximum in control cells and at 20 min in cytokine-treated cells. (n=3; \*\*\*, P<0.001, \*\*, P<0.01, \*, P<0.05 compared with vehicle-treated cells).

**FIGURE 2.** B2R-mediated NO production is more sensitive to inhibition by eNOS-selective inhibitor (L-NNA) than nNOS-selective inhibitor (N<sup>w</sup>-propyl-L-arginine) and is attenuated in cells electroporated

with siRNA targeting eNOS. A. Western analysis was used to detect eNOS, nNOS, iNOS and  $\beta$ -actin (loading control) protein expression. B. B2R-mediated NO production measured in cytokine-treated HLMVEC pretreated with increasing doses of L-NNA and  $N^w$ -propyl-L-arginine in the presence of 1  $\mu$ M DALKD and 20  $\mu$ M MGTA prior to stimulation with BK. Data are expressed as mean NO production (% of vehicle)  $\pm$  SE achieved at 20 min. (n=3; \*, P<0.05, \*\*, P<0.01, \*\*\*, P<0.001 compared with vehicle-treated cells). C. HLMVEC were transfected by electroporation (EP) with vehicle (Mock EP), 100 nM eNOS siRNA or 100 nM negative control (NC) siRNA. Post-transfection (48-72 h), cells were cytokine treated and B2R-mediated NO production was measured in the absence or presence of 4  $\mu$ M L-NNA or 4  $\mu$ M 1400W. D. HLMVEC were electroporated as described above. Receptor-independent NO production was measured in control HLMVEC in the absence or presence of 4  $\mu$ M L-NNA or 4  $\mu$ M 1400W prior to stimulation with 10  $\mu$ M A23187. Data are expressed as mean [NO], nM  $\pm$  SE achieved at 20 min. (n=3; \*\*, P<0.01, \*, P<0.05, n.s.=not significant compared with vehicle-treated cells)

**FIGURE 3.** Time course of cytokine-induced change in the pattern of B2R-mediated NO production in HLMVEC pretreated without (0 h) or with 5 ng/mL IL-1 $\beta$  and 100 U/mL IFN- $\gamma$  for 2 h, 6 h, 10 h and 16 h prior to stimulation with 100 nM BK.

**FIGURE 4.** B2R-dependent eNOS activation is mediated by divergent signaling pathways in control and cytokine-treated cells. B2R-mediated NO production measured from control and cytokine-treated cells pretreated with vehicle, calcium chelator (BAPTA-AM; 25  $\mu$ M),  $G\alpha_{i/o}$  inhibitor (PTx; 1.5  $\mu$ g/mL, 3 h), Akt inhibitor (SH-6; 15  $\mu$ M or MK2206; 5  $\mu$ M) and MEK1/2 inhibitors (PD98059; 50  $\mu$ M, or U0126; 10  $\mu$ M), for 30 min (unless otherwise indicated) at 37°C. Cell-type and agonist conditions are as follows: A. Control and cytokine-treated HLMVEC stimulated with 100 nM BK in the presence of 1  $\mu$ M DALKD and 20  $\mu$ M MGTA. B. Control and cytokine-treated HEK-B2R/eNOS stimulated with 100 nM BK in the presence of 1  $\mu$ M DALKD and 20  $\mu$ M MGTA. C. Control and cytokine-treated HLMVEC stimulated with 100 nM BK-analog. Data are expressed as mean NO concentration (% of vehicle)  $\pm$  SE achieved at the peak maximum in control cells and at 20 min in cytokine-treated cells. (n=3; \*\*\*, P<0.001, \*\*, P<0.01, \*, P<0.05 compared with vehicle-treated cells).

**FIGURE 5.** eNOS is activated independent of B2R-mediated increases in  $[Ca^{2+}]_i$ . A. Comparison of tracings of real time measurement of BK-stimulated NO production in control and cytokine-treated HLMVEC pre-incubated with vehicle or 25  $\mu$ M BAPTA (30 min at 37°C) in the presence of 1  $\mu$ M DALKD and 20  $\mu$ M MGTA. B. Cytokine-treated HLMVEC were stimulated with 2  $\mu$ M thapsigargin (TG) or 100 nM BK and [NO] was measured at 20 min. NO generation was also measured in cells stimulated with BK for 20 min that were pretreated with TG (20 min at 37°C) in the absence and presence of 25  $\mu$ M BAPTA-AM (30 min at 37°C). Data are expressed as mean [NO], nM  $\pm$  SE achieved at 20 min. C. B2R-mediated NO production was measured in control and cytokine-treated HLMVEC pre-incubated in  $Ca^{2+}$ -free media in the presence of vehicle or 50  $\mu$ M 2-APB. D. B2R-mediated increase in  $[Ca^{2+}]_i$  was measured in control and cytokine-treated HLMVEC pretreated with 1  $\mu$ M DALKD and 20  $\mu$ M MGTA 30 minutes prior to stimulation with 1  $\mu$ M BK. The tracings show mean  $\pm$  S.D. obtained from the responding population of cells (~20-30%) from 3 independent experiments. The results are shown as the ratio of fluorescence intensities excited at 340 and 380 nm. E. B2R-mediated increase in  $[Ca^{2+}]_i$  was measured in cytokine-treated HLMVEC pretreated with vehicle or 1.5  $\mu$ g/mL of PTx (3 h at 37°C) prior to stimulation with 1  $\mu$ M BK in the presence of 1  $\mu$ M DALKD and 20  $\mu$ M MGTA.

**FIGURE 6.** Cytokine treatment increases basal eNOS affinity for calcium-calmodulin ( $Ca^{2+}$ -CaM) and enhances L-Arg stimulated eNOS activation. A. (Top) Representative immunoblot (IB) showing the association between CaM and total eNOS immunoprecipitated (IP) from unstimulated (w/o BK) control and cytokine-treated HLMVEC. Total eNOS and CaM protein expression was analyzed in total cell

lysates and non-specific binding was evaluated using the proper IgG and bead controls. (*Bottom*) Densitometry data expressed as mean fold increase relative to basal  $\pm$  SE. (n=4; \*, P<0.05 compared with basal). B. (*Top*) Real time NO measurements of substrate-depleted control (*left*) and cytokine-treated (*right*) HLMVEC stimulated with 1 mM L-Arg in the absence (trace 1) or presence of 4  $\mu$ M 1400W without (trace 2) or with 4  $\mu$ M L-NNA (trace 3). (*Bottom*) Data are expressed as mean NO concentration (% of vehicle)  $\pm$  SE achieved at 20 min. (n=3; \*\*\*, P<0.001, \*\*, P<0.01, \*, P<0.05 compared with vehicle-treated cells, and #, P<0.05 compared with cells pretreated with 1400W).

**FIGURE 7.** B2R-mediated NO production is dependent on MEK1/2 and subsequent JNK1/2 but not ERK1/2 activation in cytokine-treated HLMVEC. B2R-mediated NO production was measured in control and cytokine-treated HLMVEC with the following treatments. A. Control or cytokine-treated HLMVEC were pretreated with vehicle or the following MEK1/2 inhibitors; 10  $\mu$ M U0126; 25  $\mu$ M PD98059 and 2  $\mu$ M CI-1040 (30 min at 37°C). Samples were pretreated with 10  $\mu$ M U0124, as a negative control for MEK1/2 inhibitor U0126. Data are expressed as mean [NO], nM  $\pm$  SE achieved at max in control cells and at 20 min in cytokine-treated cells. (n=3; \*\*\*, P<0.001, \*\*, P<0.01, \*, P<0.05 compared with vehicle-treated cells). B. Cells were pretreated with vehicle, ERK1/2 inhibitor (50  $\mu$ M FR180204) and ERK1/2 inhibitor negative control (50  $\mu$ M FR180289). (n=3; n.s.=not significant, compared with cells treated with negative control). C. As an ERK1/2 inhibitor positive control, cytokine-treated HLMVEC were pretreated with vehicle or 50  $\mu$ M FR180204 and then stimulated with 100 nM kinin B1 receptor (B1R) agonist DAKD (*top*) and the effect on NO production was compared with cells stimulated with 100 nM BK (*bottom*). D. Cells were pretreated with vehicle, 20  $\mu$ M JNK Inhibitor II (SP600125) or 10  $\mu$ M JNK Inhibitor VIII. (n=3; \*\*, P<0.01, compared with vehicle-treated cells). Cytokine-treated (E) or control (F) HLMVEC were electroporated (EP) with 100 nM JNK1/2 siRNA or 100 nM negative control (NC) siRNA. (n=3; \*\*\*, P<0.001, n.s.=not significant compared with NC siRNA). Total-JNK1/2 (T-JNK1/2) and total-eNOS protein expression were measured by Western analysis from control and cytokine-treated HLMVEC total cell lysates.

**FIGURE 8.** BK stimulates  $G\alpha_i$  and MEK1/2-dependent JNK1/2 phosphorylation in cytokine-treated HLMVEC. A. Total cell lysates collected from control and cytokine-treated HLMVEC stimulated with 100 nM BK for various times. JNK1/2 activation was detected with phospho-JNK (Thr183/Tyr185) antibody and was normalized to total-JNK protein expression. B. B2R-mediated JNK1/2 phosphorylation was analyzed in total cell lysates collected from cytokine-treated HLMVEC pre-incubated with vehicle or 1.5  $\mu$ g/mL PTx (3 h at 37°C). C. Western analysis of BK-stimulated JNK1/2 and ERK1/2 phosphorylation in the absence or presence of 10  $\mu$ M U0126 (15 min at 37°C). D. HLMVECs were electroporated with 100 nM MEK1/2 siRNA or 100 nM negative control (NC) siRNA. Between 48-72 h, HLMVEC were treated with cytokines (16-24 h) and then stimulated with 100 nM BK for various times. Total-MEK1/2 (T-MEK1/2) and JNK1/2 phosphorylation (P-JNK1/2) were assessed by Western blot analysis. Densitometry data for A-D are expressed as mean fold change relative to basal  $\pm$  SE. (n=3; \*\*\*, P<0.001, \*\*, P<0.01, \*, P<0.05 compared with basal).

**FIGURE 9.** B2R-mediated eNOS phosphorylation at Ser<sup>1177</sup>, Thr<sup>495</sup> and Ser<sup>114</sup> is independent of JNK1/2 activation and requires increased [Ca<sup>2+</sup>]<sub>i</sub>. A. Cytokine-treated HLMVEC pre-incubated with 1  $\mu$ M DALKD and 20  $\mu$ M MGTA and then stimulated with 100 nM BK for various times. Total cell lysates were prepared and immunoblotted with total-eNOS and phospho-specific eNOS antibodies directed against pSer<sup>1177</sup>, pThr<sup>495</sup>, pSer<sup>615</sup>, pSer<sup>633</sup> and pSer<sup>114</sup>. Representative immunoblots are shown. B. Densitometry of blots from three independent sets of lysates. Data are expressed as mean fold change relative to basal  $\pm$  SE. (n=3; \*\*\*, P<0.001, \*\*, P<0.01, \*, P<0.05 compared with basal). C. Cytokine-treated HLMVEC were pre-incubated in the absence or presence of 25  $\mu$ M BAPTA-AM, 20  $\mu$ M SP600125 (JNK inhibitor II) or vehicle for 30 min at 37°C followed by stimulation with 100 nM BK in

the presence of 1  $\mu\text{M}$  DALKD and 20  $\mu\text{M}$  MGTA. Total cell lysates were immunoblotted with total-eNOS and phospho-specific eNOS antibodies directed against pSer<sup>1177</sup> and pSer<sup>114</sup>. Representative immunoblots are shown. D. Densitometry of blots from three independent sets of lysates. Data are expressed as mean fold change relative to basal  $\pm$  SE. (n=3; \*\*\*, P<0.001, \*\*, P<0.01 compared with basal).

**FIGURE 10.** B2R-mediated NO production slows wound healing in cytokine-treated HLMVEC but enhances wound healing in control HLMVEC. Wound healing was assessed using an *in vitro* scratch assay technique. A. Images of cell migration into the cell-free region were recorded using a phase-contrast microscope at 0 h and 12 h post-treatment with 1  $\mu\text{M}$  BK or vehicle (DMEM/F-12) in the absence or presence of B2R antagonist HOE-140 (10  $\mu\text{M}$ ) or eNOS inhibitor L-NNA (4  $\mu\text{M}$ ). B. The total open area remaining was quantified using Image J Software. Data are expressed as percentage of wound closure in comparison with that of the control (vehicle) and shown as mean  $\pm$  SE. (n=3; \*\*, P<0.01, \*, P<0.01 compared with vehicle and ###, P<0.001, ##, P<0.01 compared with BK-stimulated cells in the absence of inhibitor. C. A bar graph representing the percentage of apoptotic (open bars) and non-apoptotic cells (solid bars). Data were collected from 75-125 cells per sample set and is expressed as mean  $\pm$  SE (n=3). Apoptosis was assessed by TUNEL staining as described in Experimental Procedures. Cytokine-treated HLMVEC were stimulated with 1  $\mu\text{M}$  BK for 12 h in the presence of 1  $\mu\text{M}$  DALKD & 20  $\mu\text{M}$  MGTA. *Positive control:* HLMVEC were treated with 50 U/mL of recombinant DNase I (DNA-specific endonuclease) prior to enzymatic labeling. *Negative control:* HLMVEC were treated in the absence of terminal deoxynucleotidyl transferase..

**FIGURE 11.** B2R-mediated NO production enhances transmigration of control HLMVEC but slows transmigration of cytokine-treated HLMVEC. The effect of BK on the migration of cytokine-treated (A) or control (B) HLMVEC was tested in a modified Boyden chamber assay in the absence or presence of 10  $\mu\text{M}$  HOE or 4  $\mu\text{M}$  L-NNA. All cells were pretreated with 1  $\mu\text{M}$  DALKD and 20  $\mu\text{M}$  MGTA prior to agonist stimulation. Results are expressed as mean fold change in migration of HLMVEC from the top to bottom side of the membrane relative to vehicle  $\pm$  S.E. (n=3; \*\*\*, P<0.001, \*\*, P<0.01, \*, P<0.05).

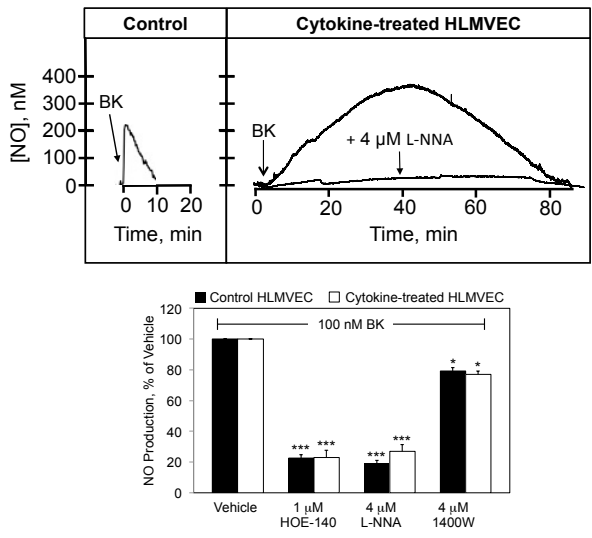
**FIGURE 12.** Scavenging ROS increases B2R-mediated NO bioavailability and impedes BK-induced delay in wound healing. A. B2R-mediated NO production measured in control (*left*) and cytokine-treated (*middle*) HLMVEC pretreated without or with 10  $\mu\text{M}$  tempol (30 min at 37°C) prior to stimulation with 100 nM BK in the presence of 1  $\mu\text{M}$  DALKD and 20  $\mu\text{M}$  MGTA. (*Right*) Real time NO measurements from cytokine-treated HLMVEC (preincubated with 4 $\mu\text{M}$  1400W) after addition of 100  $\mu\text{M}$  tempol. B. B2R-mediated NO production measured in control and cytokine-treated HLMVEC pretreated without or with 100 U/ml PEG-SOD (30 min at 37°C) prior to stimulation with 100 nM BK in the presence of 1  $\mu\text{M}$  DALKD and 20  $\mu\text{M}$  MGTA. Data are expressed as mean NO concentration  $\pm$  SE achieved at 20 min. (n=3; \*, P<0.05 compared with vehicle-treated cells). C. Using the *in vitro* scratch assay technique, wound closure was monitored in cytokine-treated HLMVEC pretreated without or with 10  $\mu\text{M}$  tempol prior to stimulation with 1  $\mu\text{M}$  BK. D. Data are expressed as percentage of wound closure compared with that of the control (vehicle) and shown as mean  $\pm$  SE. (n=3; \*, P<0.05, \*\*, P<0.01).

**FIGURE 13.** Proposed signaling pathway for basal and BK-mediated eNOS activation in inflamed endothelium. A. In healthy ('control') endothelial cells, eNOS is inactive and does not interact with calmodulin (CaM) at resting Ca<sup>2+</sup> levels. Conversely, eNOS associates with CaM at resting Ca<sup>2+</sup> levels in HLMVEC pretreated with IL-1 $\beta$  and IFN- $\gamma$  ("cytokine treated") for 16-24 h. Consequently, L-Arg stimulated eNOS activation is enhanced in cytokine treated but not control cells. B. In cytokine-treated HLMVEC, prolonged B2R-dependent NO production is mediated by PTx-sensitive G $\alpha_{i/o}$ , MEK1/2-dependent JNK1/2 activation. The mechanism by which JNK1/2 regulates eNOS activation has yet to be

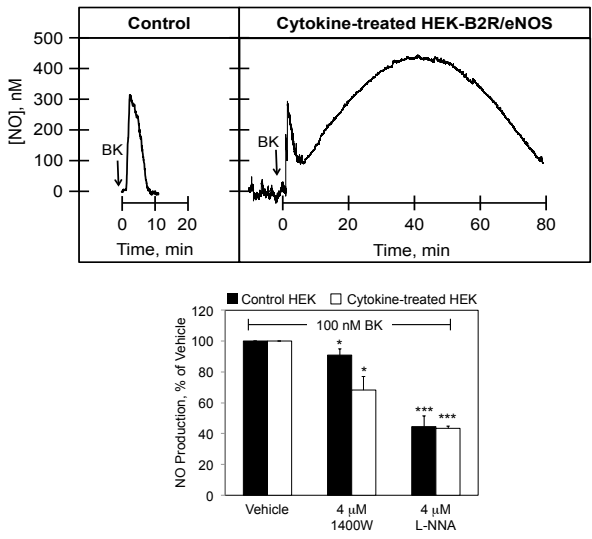
determined, but might involve JNK1/2-dependent phosphorylation of eNOS in a region that facilitates  $\text{Ca}^{2+}$ -CaM binding, thereby reducing its dependence on increases in  $[\text{Ca}^{2+}]_i$ . B2R-mediated NO production inhibits migration of cytokine-treated HLMVEC, which was partially reversed in the presence of the ROS scavenger tempol. Impaired cell migration could prevent proper angiogenesis and wound healing.

FIGURE 1.

A



B



C

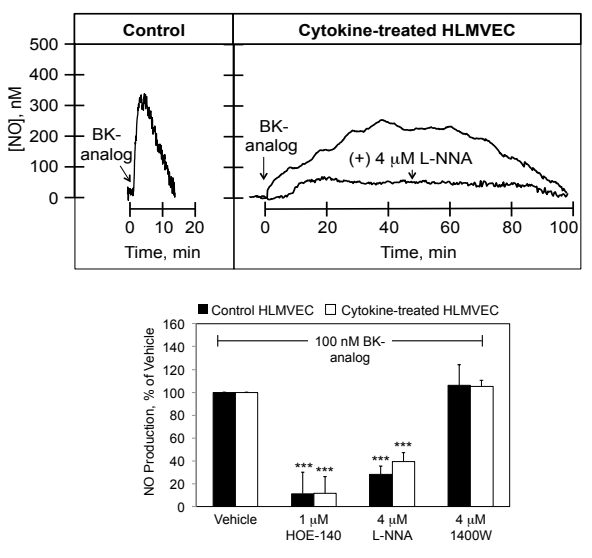
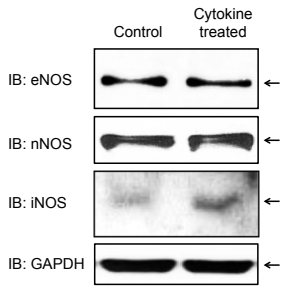
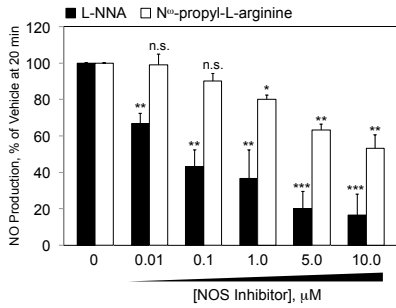


FIGURE 2.

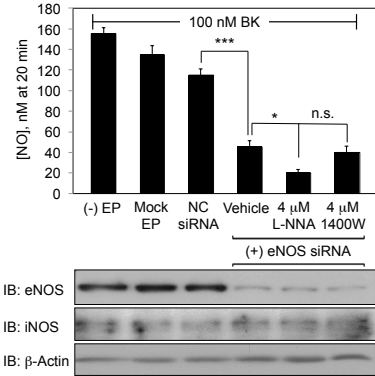
A



B



C



D

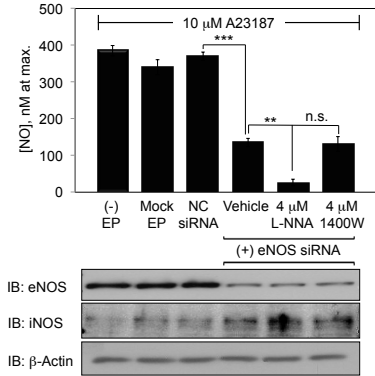


FIGURE 3.

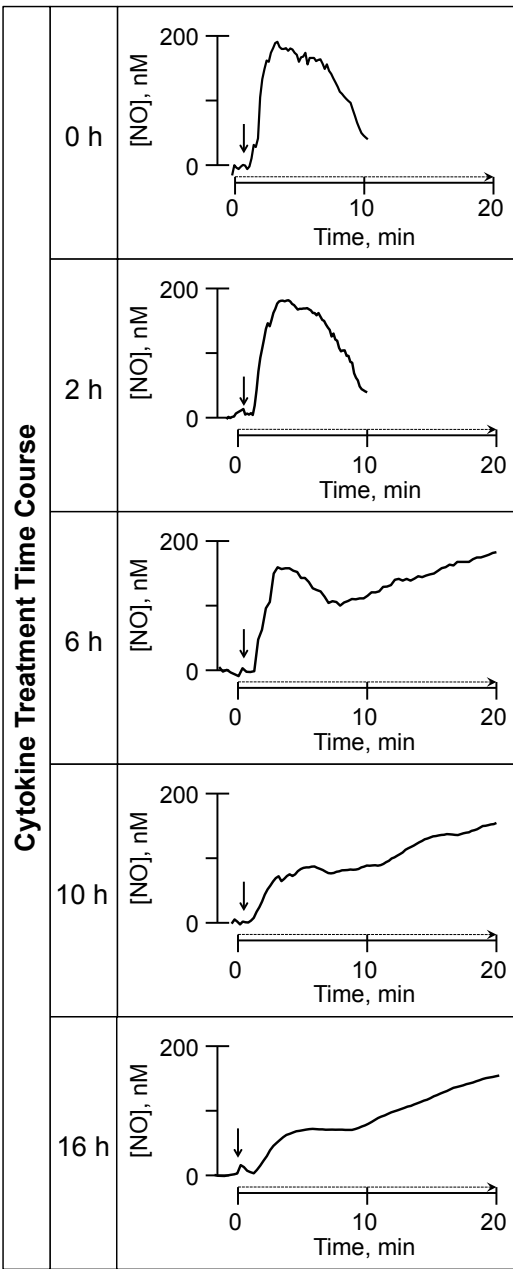
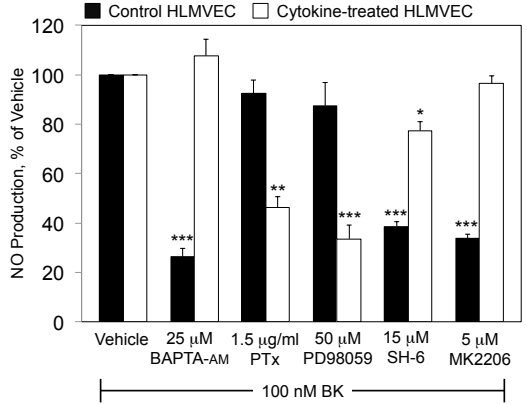
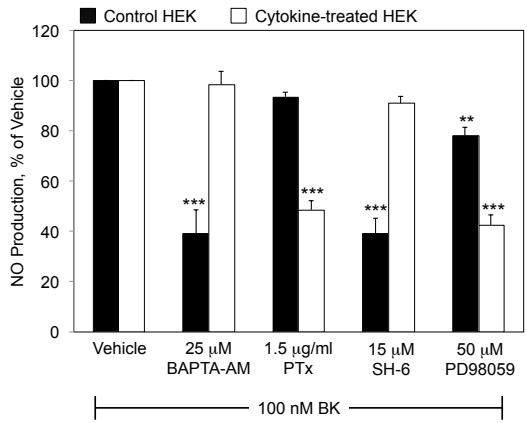


FIGURE 4.

A



B



C

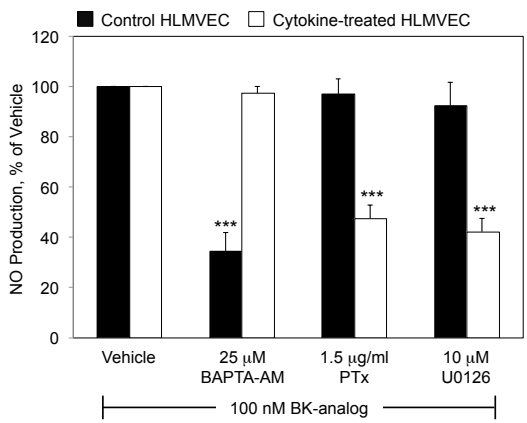


FIGURE 5.

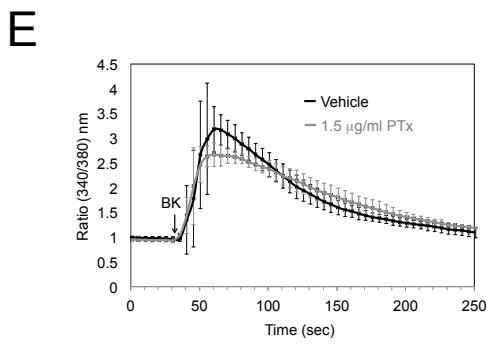
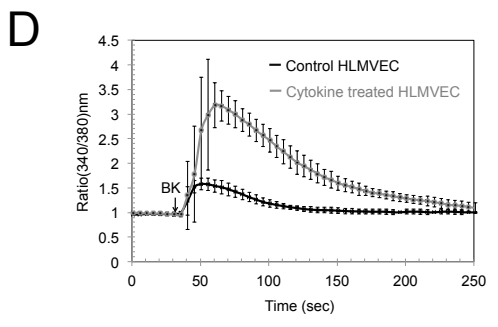
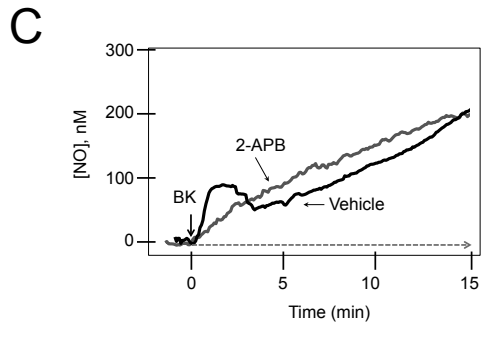
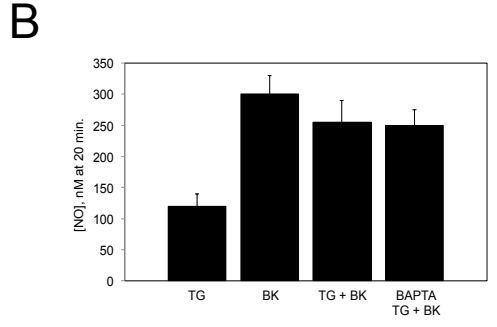
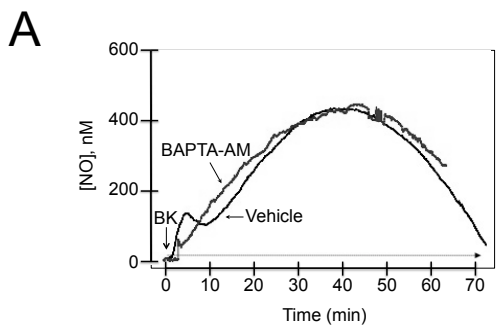
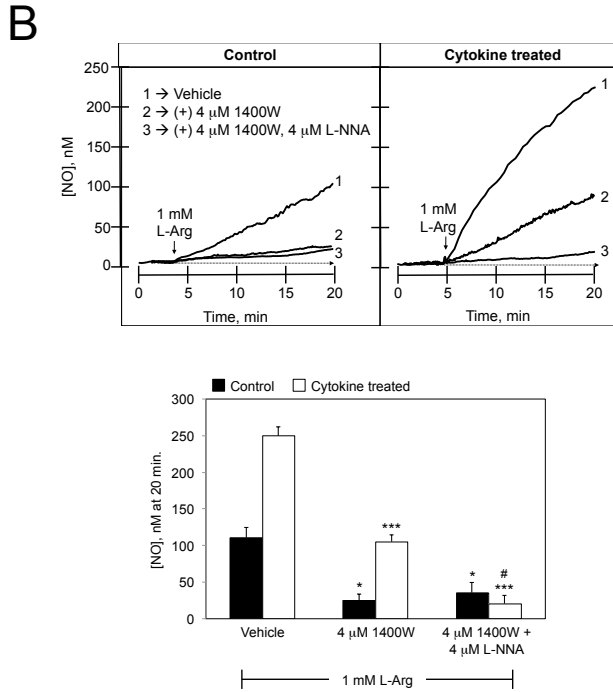
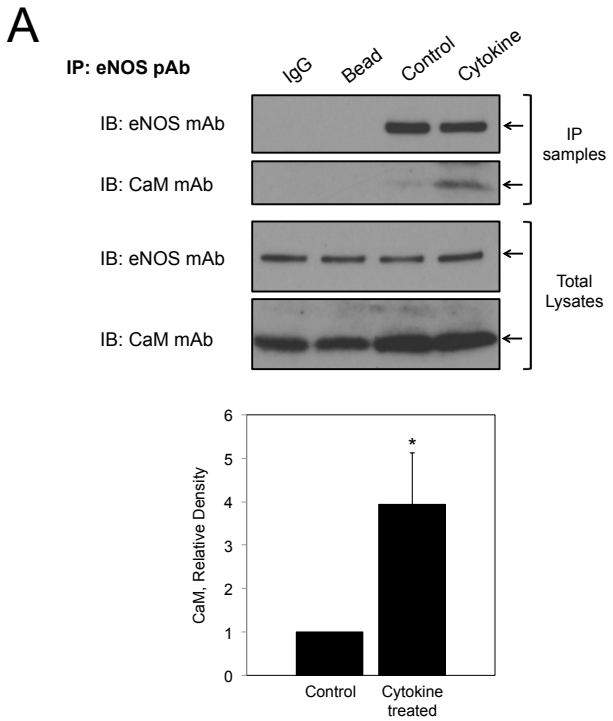
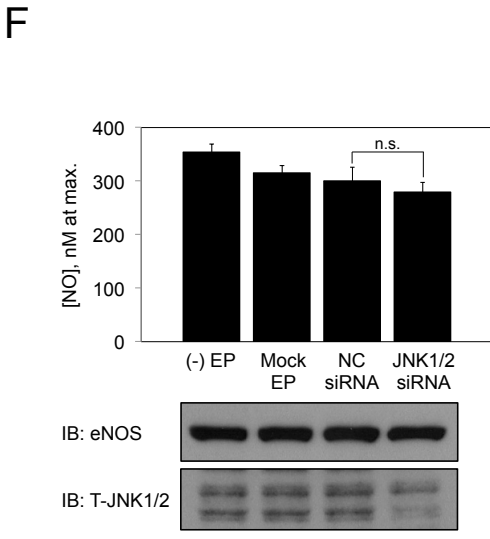
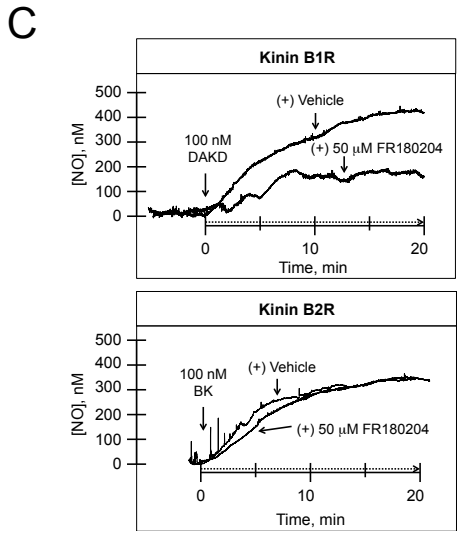
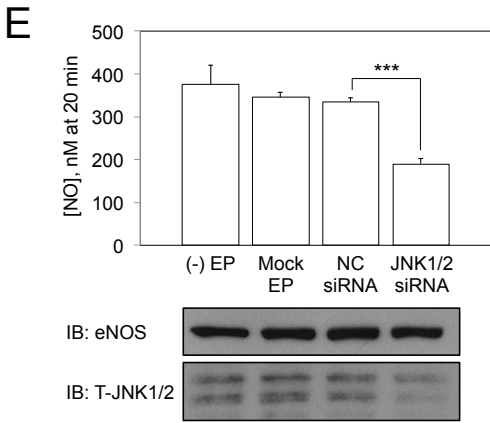
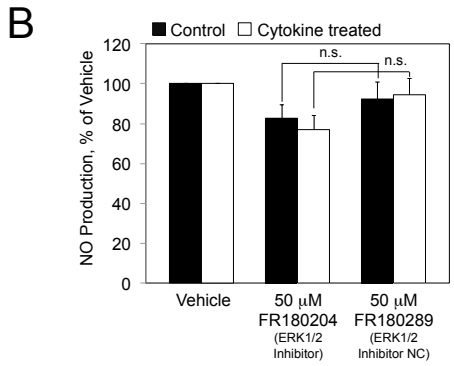
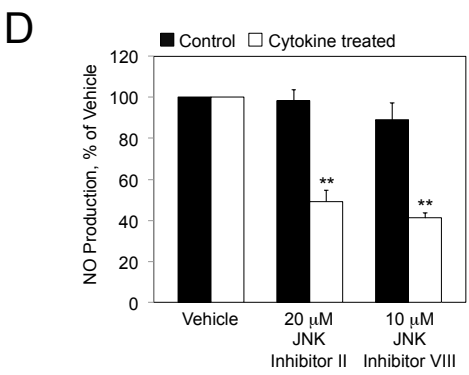
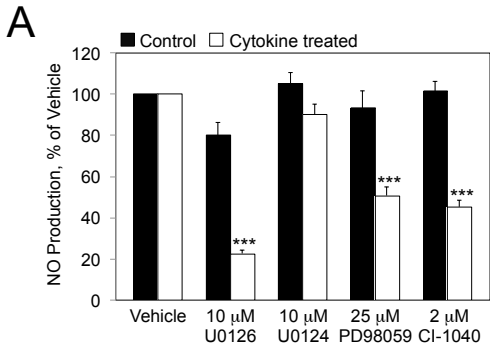


FIGURE 6.



**FIGURE 7.**



**FIGURE 8.**

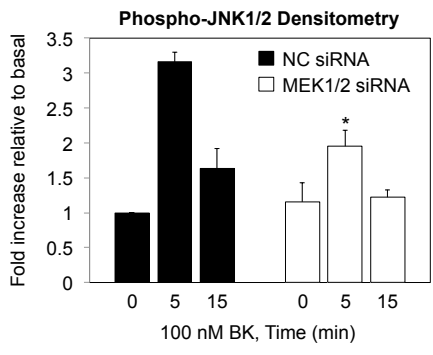
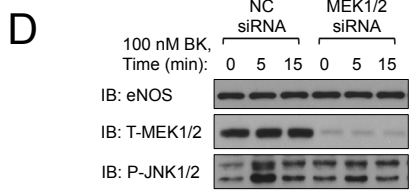
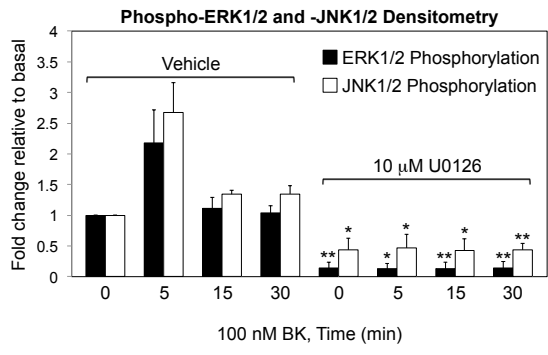
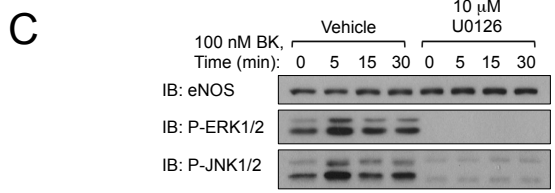
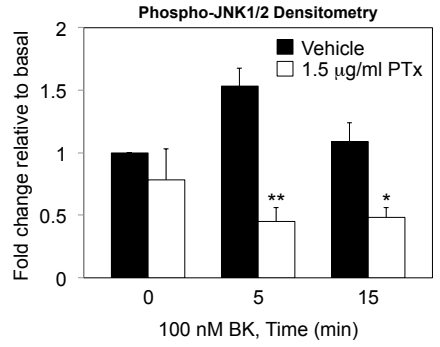
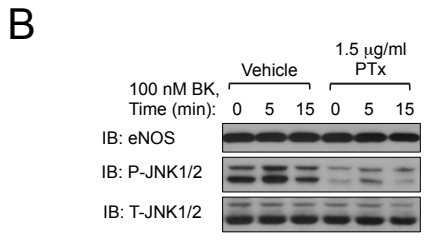
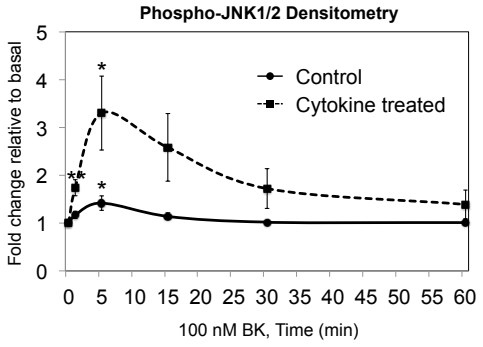
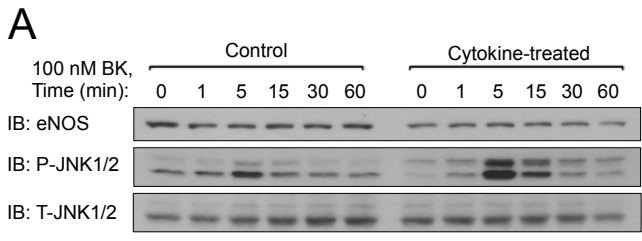


FIGURE 9.

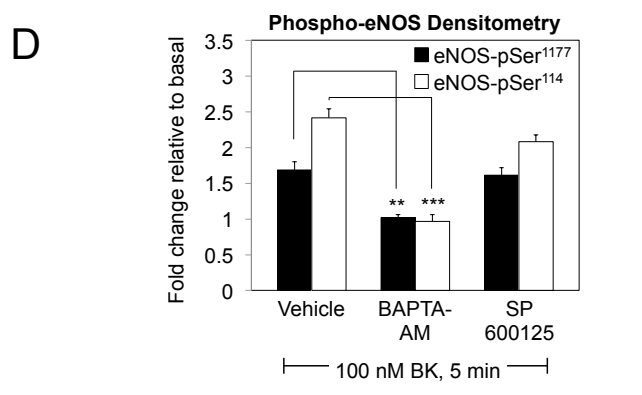
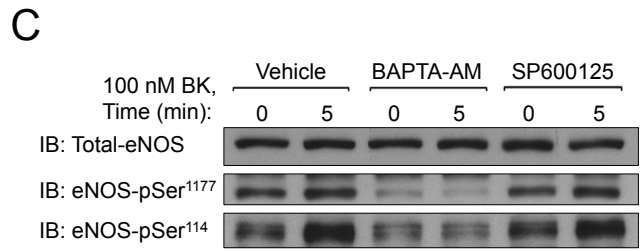
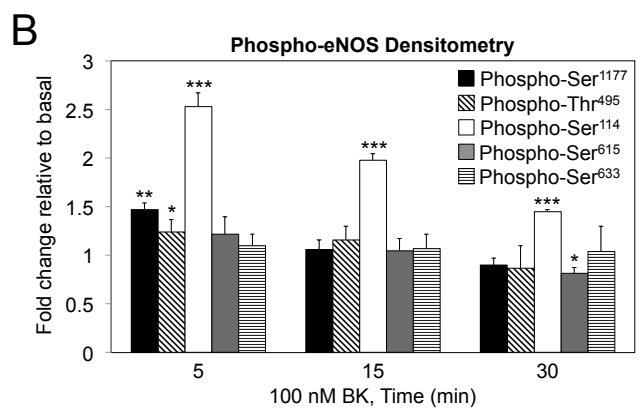
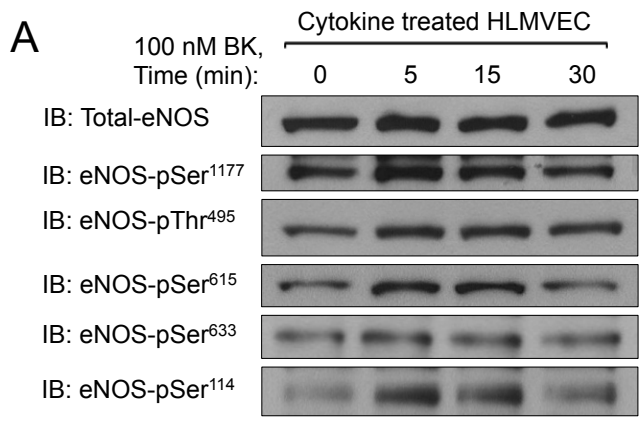


FIGURE 10.

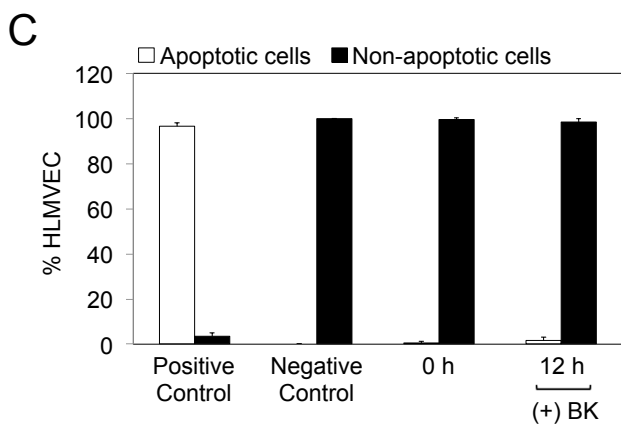
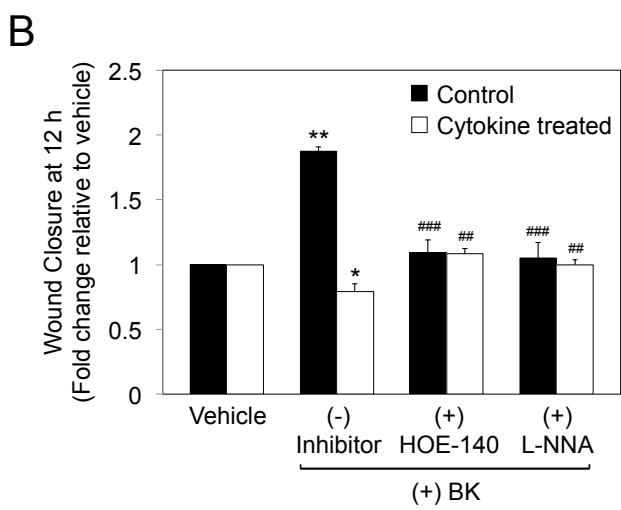
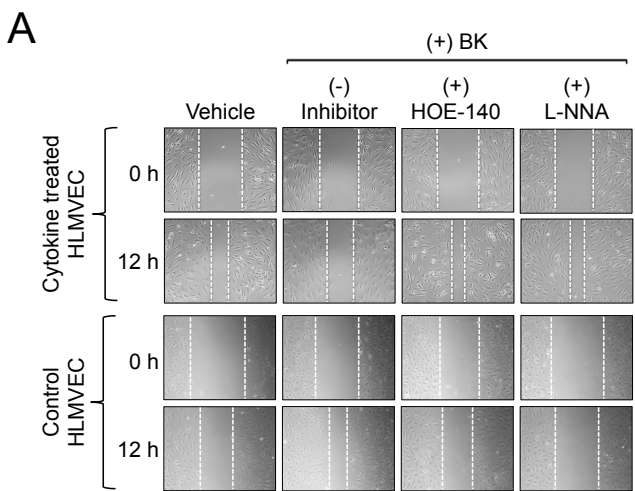
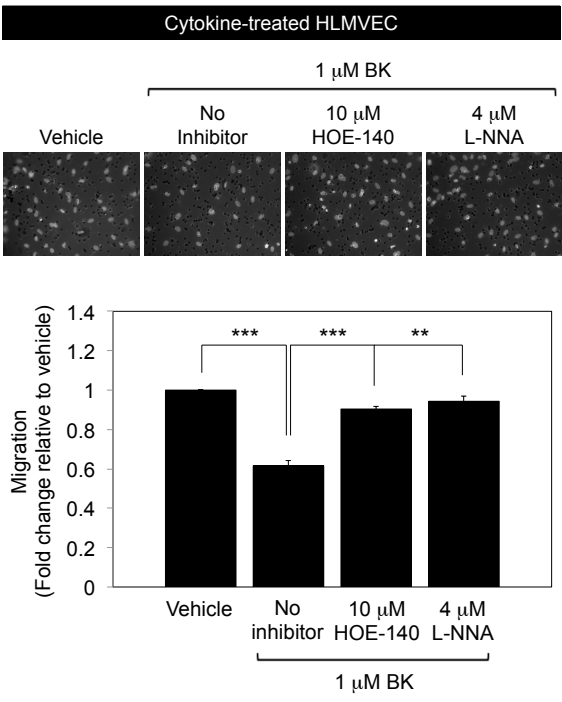


FIGURE 11.

A



B

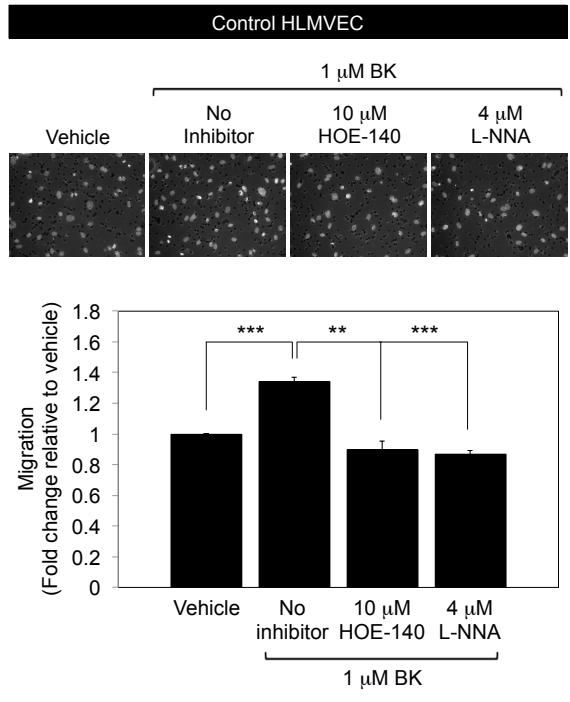
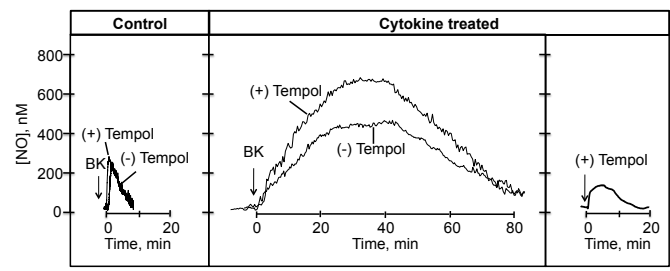
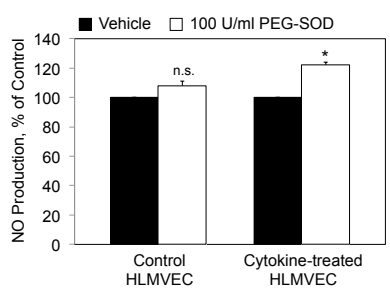


FIGURE 12.

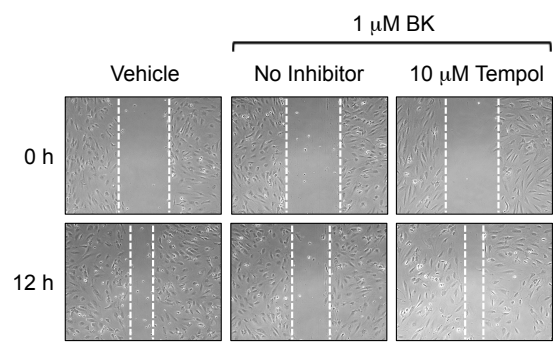
A



B



C



D

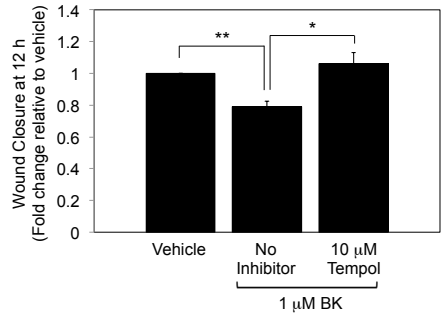
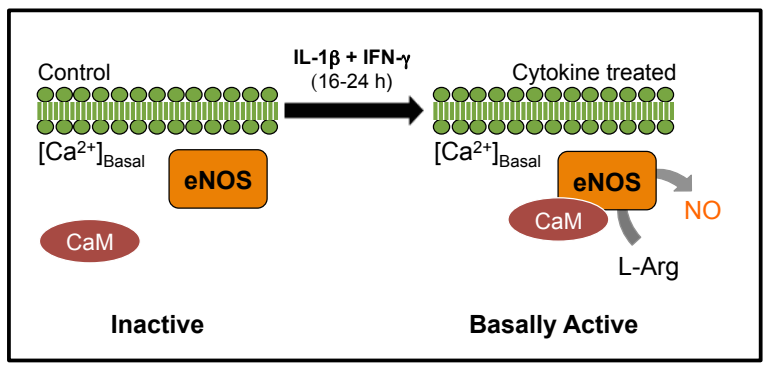


FIGURE 13.

A



B

